Field Measurements of Inhomogeneous Wave Conditions in Bjørnafjorden

Zhengshun Cheng[1], Erik Svangstu[2], Zhen Gao[3], and Torgeir Moan[4]

[1]Postdoctoral Fellow, Department of Marine Technology, Centre for Ships and Ocean Structures (CeSOS), Centre for Autonomous Marine Operations and Systems (AMOS), Norwegian University of Science and Technology (NTNU), Trondheim, 7491, Norway (corresponding author). Email: zhengshun.cheng@gmail.com

[2]Engineer, Norwegian Public Roads Administration, Leikanger, 6863, Norway. Email: erik.svangstu@vegvesen.no

[3]Professor, Department of Marine Technology, CeSOS and AMOS, Norwegian University of Science and Technology (NTNU), Trondheim, 7491, Norway. Email: zhen.gao@ntnu.no

[4]Professor, Department of Marine Technology, CeSOS and AMOS, Norwegian University of Science and Technology (NTNU), Trondheim, 7491, Norway. Email: torgeir.moan@ntnu.no

ABSTRACT

Due to the complex topography in a fjord, wave conditions differ from those of ocean waves. In this study, characteristics of wave conditions in Bjørnafjorden, Norway were thoroughly investigated based on field measurements. Bjørnafjorden is about 4600 m wide and more than 500 m deep, with a complex hydrography and topography. Three Datawell wave riders (DWRs) were deployed to measure the wave data. Due to two ferry routes nearby, the measured raw data are found to be influenced by ship waves. A band-pass filter based on wavelet and inverse wavelet analyses was thus proposed and developed to detect and remove ship waves from raw data. The wave data analyzed was measured in approximately 19 months. The wave condition measured by each DWR is characterized by several parameters, such as significant wave height, average zero up-crossing period, and dominant direction. The value of each wave parameter at each DWR usually differ,

which indicates that the wave field in Bjørnafjorden is inhomogeneous. The statistical values of these parameters among the three DWRs present to some extent correlation. Their distribution cannot be fitted by a suitable distribution function unless more data are available. The coherence among the three DWRs are fairly low.

Keywords: wave conditions, fjord, field measurement, ship waves, inhomogeneous waves.

BACKGROUND

The Norwegian Public Road Administration (NPRA) has a goal to develop an improved and continuous coastal highway route E39 between Kristiansand and Trondheim. Several deep and wide fjords are to be connected by floating bridges, instead of ferries. Such an ambitious project is extremely challenging. One of the challenges is due to the unique environmental conditions at each fjord where a floating bridge is to be used. This study aims to illustrate characteristic wave conditions in a fjord based on field measurements.

Waves in a fjord commonly consist of swell from the ocean and wind waves generated by local winds. Due to the complex topography in a fjord, the wave condition is spatially inhomogeneous, which might imply different wave spectra, wave directions and phase angles between individual waves across the fjord. This is quite different from ocean waves and is of great interest.

The fjord considered in this study is the Bjørnafjorden in Hordaland county, Norway. It has a width of about 4600 m and a depth of more than 500 m. The location and surroundings of the Bjørnafjorden is shown in Figs. 1(a) and 1(b). The local bathymetry is demonstrated in Fig. 1(c). A floating bridge is to be designed and built to cross it. To design a reliable floating bridge, the wave condition plays a very important role and should be properly estimated.

To characterize the wave condition in Bjørnafjorden, both numerical simulations and field measurements have been carried out. The numerical simulations were conducted by Norconsult (Lothe and Musch 2015) using the STWAVE (Steady-State Spectral Wave Model) (Massey et al. 2011) software, and by SINTEF using the SWAN (Simulating WAves Nearshore) model embedded in WorldWaves software (Stefanakos 2015). By using STWAVE and SWAN, both swell and wind waves were modeled, but separately. Wind waves were based on hindcast wind data from 1979 to 2015, while swell was based on offshore hindcast data from 1957 to 2014. Numerical results by Norconsult (Lothe and Musch 2015) indicated that swell can reach the three buoy locations, but the significant wave height of swell is very small (100 year value of significant wave height is about 0.4m (SVV 2016)) and the local waves at the three buoy locations are mainly wind generated. Since STWAVE and SWAN are developed based on the phase-averaged energy balance equation, they can only provide the wave frequency spectra and directional spectra at a specified point; however, cross spectra between different points in Bjørnafjorden cannot be obtained. Hence, features of the inhomogeneous wave field cannot be completely captured by numerical simulations using STWAVE or SWAN. However, these features are important, because they provide the basis for a proper representation of the wave field and a reasonable assessment for wave load effect of a long floating bridge across the fjord. More complex models, such as Boussinesq type models, can well predict the inhomogeneous wave field, but they are extremely computationally expensive.

The field measurements were performed by DHI Norway (DHI 2016). The present study is based on analysis of measured wave data to provide some insights about the wave condition in Bjørnafjorden. Three Datawell Wave Riders (DWRs) were deployed in Bjørnafjorden to record the time series of wave buoy motions. Based on recorded time series, not only wave spectra and directional spectra, but also cross spectra among the measurement points can be estimated. Therefore, the inhomogeneous wave field can be to some extent captured. However, it should be noted that the cross spectra can only be estimated between locations of these three wave buoys.

In this study, the measured wave data in the fjord were analyzed to reveal the wave condition in Bjørnafjorden. Wave conditions at these three DWRs were estimated by analyzing wave frequency spectra and directional spectra. They are represented by several wave parameters, such as significant wave height, average zero up-crossing period, and dominant direction etc. The spatial variation of these parameters at the three DWRs can reveal the feature of the inhomogeneous wave field. The inhomogeneous feature was then identified by analyzing correlation of these parameters and coherence of wave spectra. Based on the inhomogeneity estimated in this study, a further study is carried out to investigate the wave load effects of a floating bridge in inhomogeneous wave conditions (Cheng et al. 2018a; Cheng et al. 2018b).

WAVE CONDITION MEASUREMENT

Three DWRs have been deployed in the Bjørnafjorden along the possible route of a floating bridge. These three DWRs are denoted as DWR1, DWR3, and DWR4. The approximate locations of these three DWRs are marked in Fig. 1(c). In this section, how the DWR measures the wave height and wave direction is first briefly described.

Assuming that the wave buoy follows the orbital motion of water particles, measuring the vertical motion of the buoy yields the wave height. This is the basic principle for the DWR to measure wave height (de Vries 2014). This is fulfilled by means of a single accelerometer. This accelerometer is mounted on a gravity-stabilized platform, which can remain almost horizontal under any sea state. Therefore, the sensitive axis of this accelerometer points in the vertical direction. After filtering and double integrating the acceleration signal, the wave elevation is thus obtained.

Wave direction is determined by measurement of the horizontal motion of the buoy and correlating this motion with the vertical motion of the buoy. The horizontal buoy motion are measured by two mutually perpendicular accelerometers in case the buoy is in the upright position. In case of tilt, the pitch and roll angles are measured by sensors and transferred to real horizontal acceleration. The horizontal motions, i.e. the north and west displacements, are thus obtained by filtering and double integrating the acceleration signals.

The wave buoy is moored to the sea bed by a catenary mooring system, as shown in Fig. 1(d). The water depth for DWR1, DWR3 and DWR4 is about 100 m, 500 m, and 500 m, respectively. The corresponding watch circles are about 70 m. It is important to be aware of the influence of mooring system on the measurement of wave height and wave direction. For waves with frequencies lower than the natural frequency of horizontal motions, the measured wave height will be affected by the mooring system (de Vries 2014).

Therefore, the measured heave, north and west displacements of the buoy is used to analyze the local wave condition. These measurements were stored every 30 minutes at a frequency of 1.28 Hz. In this study, the field measurement data from Feb. 16 to Oct. 31 in 2016 and from January 1 to October 31 in 2017 were analyzed.

As shown in Fig. 1(c), there are two ferry routes crossing the Bjørnafjorden, one connecting Sandvikvåg and Halhjem and the other connecting Våge and Halhjem. The passing ferries cause wave trains, which will be also recorded by the DWRs. Hence, the measured wave data include swell, wind waves, and ship generated waves. To analyze the wave condition in Bjørnafjorden, the ship waves should be properly separated and removed from the measured raw data.

IDENTIFICATION AND REMOVAL OF SHIP WAVES

Ship waves

Ship generated waves have been investigated by many researchers. A passing ship can generate a complex system of diverging waves and a transverse wave, known as a Kelvin wave pattern (Newman 1977). The wave periods of the wave trains are related to the ship speed U and are given by (Schroevers et al. 2011)

$$T = U\cos(\theta)\frac{2\pi}{g} \tag{1}$$

where θ is equal to $35°16'$ and g is the gravitational acceleration. The wave height can also be estimated based on the following empirical relation (Schroevers et al. 2011).

$$\frac{H}{h} = \zeta\left(\frac{l}{h}\right)^{-1/3}\left(\frac{U}{gh}\right)^{4} \tag{2}$$

in which H is the wave height, h the local water depth and l the distance of the wave to the sailing line of a ship. ζ represents the shape (sleekness) of the vessel, and is a constant value for a given vessel. Hence, the height of ship waves diminishes with the cubic root of distance l.

Ferries travel between Sandvikvåg and Halhjem every 30 minutes in daytime. Given the distance and approximate duration, the average speed for ferries is estimated and accordingly the periods of waves caused by ferries are calculated based on Eq. 1, as given in Table 1. Since the raw wave data from the DWR is stored every 30 minutes, most raw wave data are thus influenced by ship waves. These ship waves should be carefully identified and removed from the raw wave data in order to achieve wave data due to swell and local winds.

To illustrate the ship waves, representative time series of raw wave elevation measured at three DWRs, containing ship waves, are plotted in Fig. 2. Transient wave groups, i.e. ship waves, are all observed in the wave elevation of the three DWRs. Wave elevation at DWR4 contains much stronger ship waves than the others, this is because the DWR4 is located much closer to the sailing line, and thus experiences stronger ship waves according to Eq. 2.

Removing ship waves from raw data

Generally speaking, ship waves have several notable characteristics. They are transient and are highly dependent on the time. Their amplitudes are strongly affected by the relative distance between the sailing line and the measuring point. Hence it is very challenging to accurately separate the ship generated waves from the total measured signals.

According to the traditional Kelvin ship wave theory (Newman 1977), it is possible to estimate the wave height at a specific point given the ship speed and trajectory. However, this approach is not efficient when a large amount of data is required to be analyzed. In addition, variations of vessel speed and changing of sailing line are not easy to be taken into consideration in this approach.

Another idea to separate ship waves is to apply a suitable filter that can reasonably capture the ship waves. Taking advantage of the strong time-frequency dependence of ship waves, Tan (2012) successfully identify ship waves from measured wave buoy data by the wavelet analysis. Four distinguishing characteristics of ship-generated waves were indicated, such as large amplitudes, low-frequency leading edge, time-frequency shift and correlated pressure and velocity fields. However, the magnitude and time series of ship waves were not provided by Tan (2012). But the time series of ship waves can be achieved by applying inverse wavelet analysis. Therefore, a band-pass filter based on wavelet and inverse wavelet analyses is proposed in this study. By using this filter, a general procedure for detecting and removing ship waves is developed. A flow chart illustrating the procedure is given in Fig. 3.

Before presenting the details of the proposed band-pass filter, basics of wavelet and inverse wavelet analyses are first briefly introduced.

Basics of wavelet analysis

Wavelet analysis is a commonly used tool for analyzing localized variations of power within a time series. For a discrete sequence x_n, its wavelet transform is given by (Torrence and Compo 1998)

$$W_n(s) = \sum_{k=0}^{N-1} \hat{x}_k \hat{\Psi}^* (s\omega_k) \, e^{i\omega_k n \delta t} \tag{3}$$

where $k = 0 \dots N-1$ is the frequency index, ω_k is the angular frequency, s is the wavelet scale, n is the localized time index, δt is the time step. $\hat{x}_k$ is the Discrete Fourier Transform (DFT) of x_n and is defined as

$$\hat{x}_k = \frac{1}{N} \sum_{n=0}^{N-1} x_n e^{-2\pi i k n/N} \tag{4}$$

$\hat{\Psi} (s\omega_k)$ denotes the normalized wavelet function at each scale s, and the (*) indicates the complex conjugate. It can be expressed in terms of basic wavelet function, as follows

$$\hat{\Psi} (s\omega_k) = \left(\frac{2\pi s}{\delta t} \right)^{1/2} \hat{\Psi}_0 (s\omega_k) \tag{5}$$

in which $\hat{\Psi}_0 (s\omega_k)$ is the Fourier transform of the basic wavelet function $\Psi_0 (t/s)$. Several commonly used basic wavelet functions are, for instance, Morlet, Paul and DOG (derivative of a Gaussian). In this study, the basic wavelet function is chosen to be Morlet.

The wavelet transform is usually complex since the basic wavelet function is in general complex. The wavelet power spectrum can thus be defined as $|W_n(s)|^2$. Reconstructing the time series is also possible when knowing the wavelet transform. More details about the wavelet and inverse wavelet analyses are described by Torrence and Compo (1998).

Band pass filter

In this study, a band pass filter based on the wavelet and inverse wavelet analyses is proposed to detect and isolate the ship waves. The main steps involved in this band pass filter is as follows.

Step 1: detecting ship waves.

Given the raw data, wavelet analysis is first conducted for the buoy heave motion to check whether ship waves are included. Based on the roughly estimated periods of ship waves, the ship waves have energy mainly located in the range of 1-2 rad/s. Hence in the spectrogram plot, ship waves are detected if a group of relatively high wavelet power spectral densities are located during 1-2 rad/s, last for several tens of seconds and present the phenomenon of time-frequency shifts. An example wavelet power spectrum that detects ship waves is illustrated in Fig. 4(a). Very high wavelet power densities are observed during 800 s to 1200 s, and they are located in the frequency range of 1-2.5 rad/s.

Step 2: Modifying the wavelet transform.

The Step 1 can only detect ship waves. Which ranges in terms of time and frequency in the spectrogram are exactly affected by ship waves is not clear yet. To identify the time and frequency ranges, a threshold value in terms of the wavelet power density is introduced. The threshold value $I_{threshold}$ is defined as

$$I_{threshold} = \mu + \beta\sigma \tag{6}$$

where μ and σ are respectively the mean value and standard deviation of the wavelet power density that are not affected by ship waves. β is a factor and is assumed to be $\beta = 4$.

In the spectrogram, ranges with wavelet power densities higher than this threshold are affected by ship waves. To approximately isolate the ship waves, these ranges are adjusted by replacing their wavelet power densities with the mean value μ. The modified spectrogram, denoted as $|W_n(s)'|^2$, can thus be obtained, as shown in Fig. 4(b). Consequently, the modified wavelet transform $W_n(s)'$ can be approximately determined by

$$W_n(s)' = W_n(s)\sqrt{\frac{|W_n(s)'|^2}{|W_n(s)|^2}} \tag{7}$$

Step 3: Reconstructing the time series.

The modified time series can now be reconstructed by applying the inverse wavelet analysis with respect to the modified wavelet transform $W_n(s)'$.

A comparison of the original reconstructed wave elevations is demonstrated in Fig. 5(a). The corresponding ship waves are determined by subtracting the original and reconstructed time series, as shown in Fig. 5(b). It can be seen that the ship waves are successfully isolated from the original raw data. Two groups of ship waves are recorded by the DWR. This is because a passing vessel will generate waves with a range of different periods. The generated waves with a larger period, i.e. longer waves, contain more energy and travel at a larger celerity; consequently, they arrive at the buoy before the shorter waves.

A comparison of the power spectra of original and reconstructed wave elevations is also presented in Fig. 6. An extremely high peak in the vicinity of 1 rad/s is observed in the power spectrum of the original wave elevation, this is mainly due to the ship waves. After applying the band pass filter, this peak is significantly reduced to a reasonable level that is comparable with other peaks in the frequency range of 2.5-4 rad/s. In addition, the power spectral densities in the range of 1.3-2.5 rad/s are also found to be adjusted. This is also due to the fact that a passing vessel will generate waves with a range of periods.

It should be noted that the proposed method makes use of the time-frequency characteristics of ship waves. It might not work well, if the background wind waves have a similar wave frequency as the ship waves. The proposed method can also be applied to a wide range of problems, in which time-frequency dependent noises in data records are required to be identified and removed.

WAVE DIRECTIONAL ANALYSIS

Directional wave spectrum

The directional wave spectrum is commonly modeled by

$$S(f,\theta) = S(f)D(f,\theta) \tag{8}$$

where $S(f)$ is the classical one-sided spectrum. $D(f,\theta)$ is the directional spreading function (DSF) satisfying $D(f,\theta) \geq 0$ for $\theta \in [0, 2\pi]$ and

$$\int_0^{2\pi} D(f,\theta)d\theta = 1 \tag{9}$$

A simple wave model, known as a cosine-2s model, is recommended by standards and rules to describe wave spreading. The cosine-2s model defines the spreading function by (DNV GL 2014)

$$D(\theta) = \frac{\Gamma(s+1)}{2\sqrt{\pi}\Gamma(s+1/2)} \cos^{2s}\left(\frac{\theta - \theta_p}{2}\right) \tag{10}$$

where s is the spreading exponent, Γ is the Gamma function, θ_p is the mean direction defined as the vector mean wave direction of the entire directional wave spectra estimate and $\left|\theta - \theta_p\right| \leq \pi$. In this study, we also introduce the dominant direction θ_0, which is defined as the direction with the highest energy integrated over all frequencies. It assumes that the directional function is independent of frequency, i.e. $D(f, \theta) = D(\theta)$.

The directional wave spectrum can be determined by field measurement. Several measurement techniques can be used, such as the single-point systems, gauge arrays or remote-sensing systems (Hashimoto 1997). The DWR used in the study is a typical single-point device.

Based on these measurements, a number of methods have been developed to estimate the directional wave spectrum or the DSF, including Fourier series decomposition, direct or statistical fitting to parametrical model, maximum entropy methods etc. Each method has different levels of performance in terms of accuracy, computational speed, and suitability for different data types. A comprehensive review of these methods is given by Benoit et al. (1997) and Young (1994). In this study, the Fourier series decomposition method (FSDM) and extended maximum likelihood method (EMLM) are used.

Fourier series decomposition method

The cosine-2s model given in Eq. 10 was originally proposed by Longuet-Higgins et al. (1963) using the FSDM. The FSDM is a simple method, in which the general directional spreading function are expressed as an angular Fourier series,

$$D(f, \theta) = \frac{1}{\pi}\left(\frac{1}{2} + \sum_{n=1}^{\infty} (A_n(f)\cos n\theta + B_n(f)\sin n\theta)\right) \tag{11}$$

where $A_n(f)$ and $B_n(f)$ are the angular Fourier coefficients at the frequency f. Based on three simultaneous wave measurements recorded at the same location, the first angular Fourier coefficient (i.e. $A_1(f)$, and $B_1(f)$) can be obtained based on the cross-spectra (Longuet-Higgins et al. 1963). Hence, the spreading exponent s and mean wave direction θ_p can be estimated from the first angular Fourier coefficients by

$$s = \frac{r}{1-r}, r = \sqrt{A_1^2 + B_1^2}, \theta_p = \tan^{-1}\frac{B_1}{A_1} \tag{12}$$

Extended maximum likelihood method

For a single-point system, a method that provides reliable estimation of directional wave spectra is the maximum likelihood methods (Benoit et al. 1997). The EMLM was thus used in this study. The MATLAB toolbox DIWASP (DIrectional WAve SPectrum analysis) developed by Johnson (2002) was used to estimate the directional wave spectrum.

The EMLM was developed by Isobe et al. (1984) by extending the maximum likelihood method (Capon 1969) to handle various kind of wave properties. In this method, the directional spectrum is assumed as a linear summation of cross-power spectra obtained from arbitrarily measured wave properties, that is

$$\hat{S}(f,\theta) = \sum_m \sum_n \alpha_{mn}(f,\theta)\phi_{mn}(f) \tag{13}$$

in which $\alpha_{mn}(f,\theta)$ and $\phi_{mn}(f)$ are the coefficient and cross power spectrum between the m- and n-th wave properties, respectively. When the m- and n-th wave properties are taken at the same point, the cross spectrum $\phi_{mn}(f)$ can be related to the directional spectrum by a general relationship, being expressed as (Hashimoto 1997)

$$\phi_{mn}(f) = \int_0^{2\pi} H_m(f,\theta)H_n^*(f,\theta)S(f,\theta)d\theta \tag{14}$$

where $H_m(f,\theta)$ is the transfer function from the wave elevation to other wave property, and the (*)

indicates the complex conjugate. Inserting Eq. 14 into Eq. 13 yields

$$\hat{S}(f,\theta) = \int_0^{2\pi} w_{mn}(\theta,\theta')S(f,\theta)d\theta' \tag{15}$$

where

$$w_{mn}(\theta,\theta') = \sum_m \sum_n \alpha_{mn}(f,\theta)H_m(f,\theta')H_n^*(f,\theta') \tag{16}$$

Eq. 15 indicates that the estimated directional spectrum $\hat{S}(f,\theta)$ is a convolution of the true directional spectrum $S(f,\theta)$ and window function $w_{mn}(\theta,\theta')$. Therefore, as the window function $w_{mn}(\theta,\theta')$ approaches the Delta function $\delta(\theta-\theta')$, this estimate will best approach the true directional spectrum. Isobe et al. (1984) proposed the following formula for estimating the directional spectrum,

$$\hat{S}(f,\theta) = \frac{\kappa}{\sum_m \sum_n H_m(f,\theta)\phi_{mn}^{-1}(f)H_n^*(f,\theta)} \tag{17}$$

in which $\phi_{mn}^{-1}(f)$ denotes the elements of the inverse of the cross-spectral matrix, and κ is determined from the condition that $\hat{S}(f,\theta)$ should satisfy Eq. 9.

Two examples showing the wave directions are demonstrated in Fig. 7 and Fig. 8. Fig. 7 corresponds to the reconstructed wave elevation shown in Fig. 5(a), the wave elevation is relatively small with a significant wave height of 0.11 m. Its power spectrum is plotted in Fig. 6. Several dominant peaks are observed in the power spectrum of reconstructed wave elevation. These peaks are also represented in the directional wave spectrum, as shown in Fig. 7. But these peaks have different main directions, making the directional spectrum very chaotic. Fig. 8 demonstrates the wave directional spectrum at the three DWRs in the case with the largest significant wave height (higher than 1.1 m) that was recorded. The corresponding wave elevation and power spectrum are shown in Figs. 9 and 10, respectively. In this case, the wind waves are developed with a fairly long fetch, resulting in only one dominant direction at each DWR. Therefore, to study the directional properties in more details, it is recommended to investigate more energetic sea state, like those illustrated in Fig. 8.

WAVE CONDITION ANALYSIS

The three DWRs were deployed in February 2016. The largest significant wave height, about 1.83m, was measured by DWR3 in December 2016. However, one DWR was hit by a passing-by vessel and did not work during November and December 2016. Measurements in November and December 2016 were thus not included in this paper because the inhomogeneous features cannot be captured by merely one DWR.

The wave data analyzed in this paper was measured from February 16 to October 31 in 2016 and from January 1 to October 31 in 2017. A total of 27024 samples should be recorded per site. However, the downtime of the DWR measurement system occurred sometimes, mainly due to incidents that either buoy or the mooring system has been hit by passing vessels, the available data that can be used for analysis are a bit less, about 24493 samples. These ship waves in the measured data were first removed by the wavelet and inverse wavelet filter described in Section 3. Power spectral analysis and directional analysis were then applied to investigate the following parameters.

- Significant wave height $H_s = 4\sqrt{m_0}$
- Average zero up-crossing period $T_z = 2\pi\sqrt{m_0/m_2}$
- Peak period T_p (inverse of the peak wave frequency defined by the maximum energy in the spectrum)
- Dominant direction θ_0 (the direction with the highest energy integrated over all frequencies)

where $m_k = \int_0^\infty \omega^k S(\omega) d\omega$, $k = 0$ or 2, and $S(\omega)$ is the power spectral density. Here the dominant direction is used because it can better represent the prevailing wave direction under low wave conditions.

Most of the recorded wave data have very small significant wave heights. Among the total data, only 3229 samples (approximately 13.2%), are identified to have a significant wave height H_s higher than 0.3 m. For each sample, the skewness and kurtosis of wave elevation at the three DWRs are analyzed. The mean values and standard deviations of the skewness and kurtosis are given in Table 2. It can be found that the mean skewness is close to 0.1 and the mean kurtosis is close to 3.1, implying that the distribution of wave elevation is symmetric and is tailed to a Gaussian distribution.

Effect of ship waves

The effect of ship waves on the wave condition measurement is first studied. As shown in Eq. 2, the ship waves recorded by the DWR are related to vessel speed, and distance between the DWR and the sailing line. Hence, the ship waves will remain in similar magnitude if the speed and route of ferries are unchanged. The typical ship waves measured by the three DWRs are demonstrated in Fig. 2. It can be expected that when the wind waves become more energetic, the magnitude of ship waves received by the three DWRs will still remain the same and thus the percentage of contribution of ship waves to the total recorded wave data will decrease. This is verified in Fig. 11(b), which plot the difference in significant wave height between the original and reconstructed wave elevations. These differences are due to ship waves and are estimated by $\Delta Hs = Hs_{org} - Hs_{rec}$. In Fig. 11, only significant wave heights higher than 0.3 m are considered. Fig. 11(a) represents the significant wave heights of reconstructed waves. By comparing Figs. 11(a) and 11(b), it can be concluded that the effect of ship waves are less important in cases with higher significant wave heights.

Wave condition in a case with largest significant wave height

To give a direct impression on the wave condition in Bjørnafjorden, the case with the largest significant wave height during the analyzed period is presented in this section. The highest significant wave height of the recorded wave data is about 1.22 m, which was measured at DWR1 at 1 am on Aug. 9, 2016. The corresponding wave elevation at the three DWRs are shown in Fig. 9. During this period, the ferries did not operate and no ship waves are detected. The waves are mainly wind generated. Power spectra of these wave elevations are shown in Fig. 10. The significant wave heights at DWR1, DWR3 and DWR4 are respectively, 1.22 m, 1.12 m and 1.10 m, and the corresponding peak periods are all 3.77 s.

Fourier series decomposition method (FSDM) was first applied to estimate the spreading exponent s and mean wave direction θ_p. The estimated s at DWR1, DWR3, and DWR4 is about 20.1, 21.6 and 21.5, respectively. The corresponding mean direction θ_p is approximately 285.5°, 296.7° and 307.0°. Then according to Eq. 10, the directional spectra can be obtained, as shown in Fig. 8.

The directional spectra were also estimated by the extended maximum likelihood method (EMLM), as shown in Fig. 8. The estimated mean direction θ_p at DWR1, DWR3, and DWR4 is about 285.0°, 292.6° and 303.6°, respectively. The estimated dominant directions θ_0 are 288°, 305° and 312° for the DWR1, DWR3 and DWR4, respectively. The dominant directions at DWR3 and DWR4 are quite close, while that at DWR1 has a deviation about 20°. The dominant directions are directly related to the wind direction. The measured wind at that time had a direction between 280° and 290°. The 10 min wind speed was about 16.3 m/s at a height of 10 m.

When comparing the results from the FSDM and the EMLM, the mean directions estimated at each DWR by these two methods are fairly close. The FSDM gives a relatively more spreading directional spectra than the EMLM. Hence, the EMLM is adopted to estimate the wave direction. Additionally, dominant direction can better represent the prevailing wave direction when the wave conditions are low; it is thus used for statistical analysis.

Statistical analysis of wave parameters

General

To provide a reasonable description of the wave condition in Bjørnafjorden, statistical analyses are conducted with respect to significant wave height H_s, peak period T_p, average zero up-crossing period T_z and dominant direction θ_0. Since waves with H_s less than 0.3 m are too small, here only those with H_s greater than 0.3 m are considered.

The significant wave heights at three DWRs for different cases have been shown in Fig. 11(a). The average zero up-crossing period T_z, peak period T_p and dominant direction θ_0 of three DWRs for different cases are presented in Fig. 12.

The average zero up-crossing periods T_z shown in Fig. 12(a) are mainly located in the range of 2 s to 3.5 s, and they increase together with the significant wave height. A sea state with a high significant wave height is usually associated with a longer zero up-crossing period. The peak periods T_p shown in Fig. 12(b) present similar trend as the zero up-crossing periods, but several very high peak period that are larger than 7 s are also observed. These high peak period are mainly due to swell from the ocean. In addition, these peaks do not significantly alter the energy distribution of power spectra, since they follow similar trend as T_z. It also implies that swell can reach the three buoy locations, but the significant wave height of swell is very small. Regarding the dominant wave direction, Fig. 12(c) indicates that these three DWRs in general have quite similar dominant wave directions. There is about 10º discrepancy between the dominant direction of DWR1 and those of DWR3 and DWR4. One possible reason is due to refraction, since the DWR1 is located in a relatively shallower water than DWR3 and DWR4. The northern shoreline may also be a contributing factor. In addition, two major dominant wave direction are observed, one from northwest (280°-330°) and one from east. The topography shown in Fig. 1(a) indicates that northwest and east are two main directions with relatively long fetch length. Therefore, winds in these two direction are thus more likely to generate larger wind waves given the same duration and mean wind speed.

More details and inherent relations of these parameters among the three DWRs are discussed in the following sections.

Correlation analysis

From long term point of view, it is of interest to investigate the correlations of the wave parameters between the three DWRs. The correlation matrices of significant wave height H_s, average zero up-crossing periods T_z, peak periods T_p and dominant directions θ_0 between the three DWRs are given in Tables. 3-14.

For cases with significant wave height larger than 0.3 m

Tables 3- 6 gives the correlation matrix of different wave parameters between the three DWRs considering cases with significant wave height larger than 0.3 m. According to Table 3, the DWR3 has positive linear relationships with the DWR1 and DWR4 in terms of H_s, while the linear relationship between the DWR1 and DWR4 is much weaker. These differences of correlation coefficients may result from the different distances between each DWR, from different local bathymetry at each DWR, and from the northern and southern shorelines. As it is marked in Fig. 1(c), the distance between DWR1 and DWR4 is about 2831 m, which is much greater than that between the DWR3 and DWR4. These separation distances are much larger than the watch circle, approximately 70 m.

Similar trends are also observed for average zero up-crossing periods T_z in Table 5 and for peak periods T_p in Table 4. The DWR3 and DWR4 have the strongest linear relationship, while the DWR1 and DWR4 have the weakest one. In general, the correlation coefficients of T_z are generally larger than that of T_p, indicating that the average zero up-crossing periods have much better linear relationship than the peak periods. The reason for this is that in cases with a relatively small significant wave height, the power spectrum of wave elevation is likely to have several dominant peaks. An example is shown in Fig. 6. In these cases, peak periods are not good parameters representing the characteristics of the spectrum. Hence only the average zero up-crossing periods T_z is considered hereinafter.

The dominant directions at three DWRs present very high correlation between each DWR, as given in Table 6. The correlation coefficients are all higher than 0.95 and are very close to 1. The high correlation of dominant direction implies that waves at the three DWRs are coming from relatively the same place.

For cases with significant wave height larger than 0.6 m

To further investigate the correlation of wave parameters under larger waves, the correlation matrix for all cases with significant wave height larger than 0.6 m are estimated and shown in Tables 7- 10. A total of 253 samples (about 1% of total recorded data) are identified to have a significant wave height greater than 0.6 m.

Compared to the correlation coefficients in Tables 3- 6 for cases with significant wave height larger than 0.3 m, the corresponding correlation coefficients given in Tables 7- 10 are in general fairly close. But some deviations are also observed, for instance, the correlation coefficient between DWR1 and DWR3 with respect to significant wave height decrease from 0.804 to 0.683. However, it should be noted that relative large uncertainty might exist because of the relatively small sample size.

For cases with dominant wave direction from northwest

According to Fig. 12(c), most of waves with significant wave height larger than 0.3 m comes from northwest. These waves are plotted in Fig. 13. For these waves, the correlation matrix of wave parameters are also analyzed and given in Tables 11- 14.

Compared to Tables 3- 6 and 7- 10, the linear relationships between the three DWRs have increased a lot with respect to significant wave height H_s and average zero up-crossing period T_z. Especially, the correlation coefficients between DWR3 and DWR4 in terms of H_s and T_z are very close to 1, implying a extremely good correlation. However, the correlation coefficients with respect to dominant direction decrease a lot; such decrease is due to the fact that only waves from northwest are analyzed.

As a whole, the wave condition parameters at DWR3, including significant wave height, average zero up-crossing periods, and peak periods, have to some extent good linear relationship between the other two DWRs. One possible reason is that the DWR3 is located between DWR1 and DWR4, as shown in Fig. 1(c). However, the linear relationship of significant wave height and average zero up-crossing periods between the DWR1 and DWR4 are fairly weak.

Distribution analysis

The distribution features of these parameters in Bjørnafjorden are studied in this section. Fig. 13 depicts the significant wave height, average zero up-crossing periods, and dominant direction at the three DWRs for all cases with significant wave height larger than 0.3 m and with dominant direction from northwest. The corresponding histogram is shown in Fig. 14.

The histograms of significant wave height at DWR1, DWR3 and DWR4 are different, as shown in Figs. 14(a), 14(b) and 14(c). It is difficult to achieve a satisfactory result by fitting the histogram with a suitable distribution function, for instance weibull distribution. Possible reasons for this are that cases with significant wave height smaller than 0.3 m are not taken into account and that the available data for this histogram are too few. Histogram of average zero up-crossing period and dominant direction at DWR3 are also shown in Fig. 14, and fitting them with a suitable distribution function is very difficult as well.

The deviations of different wave parameters are also of interest and studied here. Since the DWR3 was deployed in the middle of DWR1 and DWR4, it was chosen as the reference. Fig. 15 shows the differences of significant wave height, average zero up-crossing period, dominant direction between DWR3 and DWR1, DWR4. Six relative deviations are also considered in this study, i.e.

- $\Delta H_{s31} = \frac{H_{sDWR3} - H_{sDWR1}}{H_{sDWR3}}$
- $\Delta H_{s34} = \frac{H_{sDWR3} - H_{sDWR4}}{H_{sDWR3}}$
- $\Delta T_{z31} = \frac{T_{zDWR3} - T_{zDWR1}}{T_{zDWR3}}$
- $\Delta T_{z34} = \frac{T_{zDWR3} - T_{zDWR4}}{T_{zDWR3}}$
- $\Delta \theta_{031} = \frac{\theta_{0DWR3} - \theta_{0DWR1}}{\theta_{0DWR3}}$
- $\Delta \theta_{034} = \frac{\theta_{0DWR3} - \theta_{0DWR4}}{\theta_{0DWR3}}$

The histogram of these deviations are shown in Fig. 16. Fitting the histograms with a suitable distribution function is also difficult here. The histograms indicates that the significant wave height at DWR3 is likely to be 18% larger than that at DWR1 and 3% smaller than that at DWR4. Difference with respect to average zero up-crossing period between the three DWRs is mainly within 5%, implying that the average zero up-crossing period tends to be the identical for the three DWRs. It should be noted that these observations are made for waves with a significant wave height larger than 0.3 m and with dominant direction from northwest.

Similar time history of wave parameters and their histograms and distribution fitting are also analyzed for cases with significant wave height larger than 0.3 m, and for cases with significant wave height larger than 0.6 m. Suitable distributions are difficult to be achieved based on the present data. More data are required.

Coherence analysis

The coherence for wave elevations between different DWRs is very important since it indicates how well the wave elevations are corresponded with each other at each frequency from the short term point of view.. Assuming the wave elevation at DWR1, DWR3 and DWR4 are denoted by η_1, η_3, and η_4, respectively. The coherence between η_i and η_j $(i \neq j; i = 1, 3, 4; j = 1, 3, 4)$ is defined as

$$Coh_{ij} = \sqrt{\frac{\left|S_{\eta_i\eta_j}\right|^2}{S_{\eta_i\eta_i}S_{\eta_j\eta_j}}} \tag{18}$$

where $S_{\eta_i\eta_i}$ and $S_{\eta_j\eta_j}$ are the power spectral densities and $S_{\eta_i\eta_j}$ is the cross spectral density.

The coherence of wave elevations between the three DWRs was first analyzed for the case with the largest significant wave height. The result is shown in Fig. 17. It can be found that the coherence level for all frequencies is fairly low.

The coherence for all cases with significant wave height higher than 0.3 m are also analyzed in this study, as shown in Fig. 18. Both the mean value and standard deviation of the coherence at each frequency are plotted. It can be found that the coherence level are all very low, and are about 0.22 for most frequencies. This implies that the wave elevations at the three DWRs have very low correspondence with each other. Small peaks in the vicinity of 1 rad/s are also observed in the coherence shown in Fig. 18. These peaks are due to the ship waves. The proposed method for removing ship waves can remove the majority of ship wave energy, but cannot remove all ship wave energy, as presented in Fig. 6 .

Similar coherence analyses are also analyzed for cases with significant wave height larger than 0.6 m, and for cases with significant wave height larger than 0.3 m and with dominant direction from northwest. The results also show that among the three DWRs, the coherence level are all very low, and are about 0.22 for most frequencies.

CONCLUDING REMARKS

This study addressed the characteristics of wave conditions in Bjørnafjorden based on field measurements. The Bjørnafjorden is about 4600 m wide and more than 500 m deep, with a complex hydrography and topography.

Three Datawell wave riders (DWRs) were deployed in Bjørnafjorden to measure the wave conditions. Since the location of DWRs was close to two ferry routes, the raw data might be influenced by ship waves. To detect and remove ship waves from raw data, a band-pass filter based on wavelet and inverse wavelet analysis was proposed and accordingly, a general procedure was developed. Ship waves can be successfully detected and removed by this band-pass filter.

The wave data analyzed was measured from Feb. 16 to Oct. 31 in 2016 and from January 1 to October 31 in 2017, in approximately 19 months. Wave directional spectra were estimated by Fourier series decomposition method (FSDM) and by extended maximum likelihood method (EMLM) using the DIWASP (DIrectional WAve SPectrum analysis) toolbox (Johnson 2002). Several wave parameters, including the significant wave height, average zero up-crossing period, peak period and dominant direction, are chosen to characterize the wave condition measured by each DWR.

The values of each wave parameter at each DWR usually differ, which indicates that the wave field in Bjørnafjorden is inhomogeneous. The inhomogeneity is due to large separation distance between DWRs, varying local bathymetry at each DWR, and northern and southern shorelines etc. The largest significant wave height was found to be 1.22 m, based on the measured data. When the significant wave height is relatively large, for instance larger than 0.3 m, the effect of ship waves is found to be insignificant.

Statistical analyses of these wave parameters in terms of correlation and histogram are also conducted. These parameters present to some extent correlation among the three DWRs. Satisfactory fitting of these histogram with a suitable distribution function can not be achieved. In addition, the coherence between the three DWRs is found to be fairly low.

As a whole, this study presents the relevant methods to analyze measured wave data to reveal the characteristic wave conditions in a fjord in Norway. It can be used to analyze wave data that are affected by transient ship waves. Though only measurements in about 19 months are analyzed, the features of waves in a fjord are captured. The inhomogeneity of wave conditions in a fjord is highlighted. But to give a wave condition for design purpose, more data are required in order to achieve a reasonable distribution fitting of these parameters and to better estimate the correlation matrix among these parameters. This can be obtained using hindcast data based on long term wind data.

For specific events, for instance under storm conditions, large-scale computational fluid dynamics (CFD) simulations are being carried out to reveal the inhomogeneous features of the wave field in the fjord. The field measurements can be used to validate the CFD simulations.

Currently the distance between DWRs are more than 1300 m, the conclusions obtained cannot be extended to a short distance (e.g. 200 m) unless an additional DWR is deployed; otherwise, large uncertainties can be expected.

ACKNOWLEDGMENT

This work was supported by the Norwegian Public Roads Administration (NPRA) and in parts by the Research Council of Norway through the Centre for Ships and Ocean Structures (CeSOS) and Centre for Autonomous Marine Operations and Systems (AMOS), at the Department of Marine Technology, NTNU, Trondheim, Norway. The support is gratefully acknowledged by the authors. The authors would like to acknowledge the NPRA for the permission to publish the measured wave data. Dr. François Beauducel is also acknowledged for writing the original matlab function facilitating the use of SRTM (Shuttle Radar Topography Mission) digital elevation model data files.

REFERENCES

Benoit, M., Frigaard, P., and Schäffer, H. A. (1997). "Analysing multidirectional wave spectra: a tentative classification of available methods." *Proc. seminar on multidirectional waves and their interaction with structures*, 131–158.

Capon, J. (1969). "High-resolution frequency-wavenumber spectrum analysis." *Proceedings of the IEEE*, 57(8), 1408–1418.

Cheng, Z., Gao, Z., and Moan, T. (2018a). "Hydrodynamic load modeling and analysis of a floating bridge in homogeneous wave conditions." *Marine Structures*, 59, 122–141.

Cheng, Z., Gao, Z., and Moan, T. (2018b). "Wave load effect analysis of a floating bridge in a fjord considering inhomogeneous wave conditions." *Engineering Structures*, 163, 197–214.

de Vries, J. (2014). "Datawell waverider reference manual, DWR-MkIII, DWR-G." *Datawell BV Oceanogr. Instrum., Heerhugowaard, Netherlands*.

DHI (2016). “Wave and current measurements in Bjørnafjorden, Hordaland, Norway.” DHI AS, Trondheim, Norway.

DNV GL (2014). “Environmental conditions and environmental loads (DNV-RP-C205).” *Det Norske Veritas AS, Oslo, Norway*.

Hashimoto, N. (1997). “Analysis of the directional wave spectrum from field data.” *Advances in Coastal and Ocean Engineering*, 3, 103–144.

Isobe, M., Kondo, K., and Horikawa, K. (1984). “Extension of MLM for estimating directional wave spectrum.” *Proc. Symp. on Description and Modeling of Directional Seas*, DHI and MMI, Copenhagen.

Johnson, D. (2002). “Diwasp, a directional wave spectra toolbox for matlab®: User manual.” WP 1601 DJ (V1. 1), Centre for Water Research, University of Western Australia.

Longuet-Higgins, M. S., Cartwright, D. E., and Smith, N. D. (1963). “Observations of the directional spectrum of sea waves using the motions of a floating buoy.” *Ocean wave spectra: Proceedings of a Conference*, 111–132.

Lothe, A. and Musch, O. (2015). “Bjørnafjorden submerged floating tube bridge: sea state simulations.” Norconsult AS, Trondheim, Norway.

Massey, T. C., Anderson, M. E., Smith, J. M., Gomez, J., and Jones, R. (2011). “Stwave: Steady-state spectral wave model user’s manual for stwave, version 6.0.” ERDC-SR-11-1, U.S. Army Engineer Research and Development Center, Vicksburg, MS.

Newman, J. N. (1977). *Marine hydrodynamics*. MIT press.

Schroevers, M., Huisman, B., Van der Wal, M., and Terwindt, J. (2011). “Measuring ship induced waves and currents on a tidal flat in the Western Scheldt estuary.” *Proceedings of the IEEE/OES/CWTM 10th Working Conference on Current Measurement Technology*, IEEE, 123–129.

Stefanakos, C. (2015). “Bridge across bjørnafjorden. metocean analyses.” SINTEF Materials and Chemistry, Trondheim, Norway.

SVV (2016). “Design basis metocean.” *Statens Vegnesen, norway*.

Tan, S. W. (2012). “Predicting boat-generated wave heights: A quantitative analysis through video observations of vessel wakes.” United States Naval Academy, Annapolis, Maryland, USA.

Torrence, C. and Compo, G. P. (1998). “A practical guide to wavelet analysis.” *Bulletin of the American Meteorological society*, 79(1), 61–78.

Young, I. (1994). “On the measurement of directional wave spectra.” *Applied Ocean Research*, 16(5), 283–294.

List of Tables

1 Two ferry routes crossing the Bjørnafjorden 27

2 The mean values and standard deviations of skewness and kurtosis of wave elevation at the three DWRs. Only waves with a significant wave height larger than 0.3 m are considered. 28

3 Correlation matrix of significant wave height H_s between the three DWRs. Only cases with significant wave height larger than 0.3 m are considered. 29

4 Correlation matrix of peak period T_p between the three DWRs. Only cases with significant wave height larger than 0.3 m are considered. 30

5 Correlation matrix of average zero up-crossing period T_z between the three DWRs. Only cases with significant wave height larger than 0.3 m are considered. 31

6 Correlation matrix of dominant direction θ_0 between the three DWRs. Only cases with significant wave height larger than 0.3 m are considered. 32

7 Correlation matrix of significant wave height H_s between the three DWRs. Only cases with significant wave height larger than 0.6 m are considered. 33

8 Correlation matrix of peak period T_p between the three DWRs. Only cases with significant wave height larger than 0.6 m are considered. 34

9 Correlation matrix of average zero up-crossing period T_z between the three DWRs. Only cases with significant wave height larger than 0.6 m are considered. 35

10 Correlation matrix of dominant direction θ_0 between the three DWRs. Only cases with significant wave height larger than 0.6 m are considered. 36

11 Correlation matrix of significant wave height H_s between the three DWRs. Only cases with significant wave height larger than 0.3 m and with dominant waves from northwest are considered. 37

12 Correlation matrix of peak period T_p between the three DWRs. Only cases with significant wave height larger than 0.3 m and with dominant waves from northwest are considered. 38

13 Correlation matrix of average zero up-crossing period T_z between the three DWRs. Only cases with significant wave height larger than 0.3 m and with dominant waves from northwest are considered. 39

14 Correlation matrix of dominant direction θ_0 between the three DWRs. Only cases with significant wave height larger than 0.3 m and with dominant waves from northwest are considered. 40

TABLE 1. Two ferry routes crossing the Bjørnafjorden

Route	Distance [km]	Duration [min]	Average speed [knots]	Wave periods [s]	Frequency [-]
Sandvikvåg-Halhjem	21.4 km	40 min	17.3 knots	4.7 s	every 30 min in daytime
Våge-Halhjem	12.1 km	35 min	11.5 knots	3.1 s	every 80 min in daytime

TABLE 2. The mean values and standard deviations of skewness and kurtosis of wave elevation at the three DWRs. Only waves with a significant wave height larger than 0.3 m are considered.

DWR ID	Skewness		Kurtosis	
	Mean	STD	Mean	STD
DWR1	0.103	0.051	3.071	0.191
DWR3	0.104	0.051	3.096	0.207
DWR4	0.103	0.054	3.144	0.206

TABLE 3. Correlation matrix of significant wave height H_s between the three DWRs. Only cases with significant wave height larger than 0.3 m are considered.

DWR ID	DWR1	DWR3	DWR4
DWR1	1	0.804	0.509
DWR3	0.804	1	0.856
DWR4	0.509	0.856	1

TABLE 4. Correlation matrix of peak period T_p between the three DWRs. Only cases with significant wave height larger than 0.3 m are considered.

DWR ID	DWR1	DWR3	DWR4
DWR1	1	0.497	0.376
DWR3	0.497	1	0.551
DWR4	0.376	0.551	1

TABLE 5. Correlation matrix of average zero up-crossing period T_z between the three DWRs. Only cases with significant wave height larger than 0.3 m are considered.

DWR ID	DWR1	DWR3	DWR4
DWR1	1	0.827	0.693
DWR3	0.827	1	0.909
DWR4	0.693	0.909	1

TABLE 6. Correlation matrix of dominant direction θ_0 between the three DWRs. Only cases with significant wave height larger than 0.3 m are considered.

DWR ID	DWR1	DWR3	DWR4
DWR1	1	0.969	0.950
DWR3	0.969	1	0.963
DWR4	0.950	0.963	1

TABLE 7. Correlation matrix of significant wave height H_s between the three DWRs. Only cases with significant wave height larger than 0.6 m are considered.

DWR ID	DWR1	DWR3	DWR4
DWR1	1	0.683	0.442
DWR3	0.683	1	0.848
DWR4	0.442	0.848	1

TABLE 8. Correlation matrix of peak period T_p between the three DWRs. Only cases with significant wave height larger than 0.6 m are considered.

DWR ID	DWR1	DWR3	DWR4
DWR1	1	0.582	0.478
DWR3	0.582	1	0.761
DWR4	0.478	0.761	1

TABLE 9. Correlation matrix of average zero up-crossing period T_z between the three DWRs. Only cases with significant wave height larger than 0.6 m are considered.

DWR ID	DWR1	DWR3	DWR4
DWR1	1	0.824	0.725
DWR3	0.824	1	0.909
DWR4	0.725	0.909	1

TABLE 10. Correlation matrix of dominant direction θ_0 between the three DWRs. Only cases with significant wave height larger than 0.6 m are considered.

DWR ID	DWR1	DWR3	DWR4
DWR1	1	0.947	0.943
DWR3	0.947	1	0.983
DWR4	0.943	0.983	1

TABLE 11. Correlation matrix of significant wave height H_s between the three DWRs. Only cases with significant wave height larger than 0.3 m and with dominant waves from northwest are considered.

DWR ID	DWR1	DWR3	DWR4
DWR1	1	0.870	0.822
DWR3	0.870	1	0.973
DWR4	0.822	0.973	1

TABLE 12. Correlation matrix of peak period T_p between the three DWRs. Only cases with significant wave height larger than 0.3 m and with dominant waves from northwest are considered.

DWR ID	DWR1	DWR3	DWR4
DWR1	1	0.473	0.444
DWR3	0.473	1	0.793
DWR4	0.444	0.793	1

TABLE 13. Correlation matrix of average zero up-crossing period T_z between the three DWRs. Only cases with significant wave height larger than 0.3 m and with dominant waves from northwest are considered.

DWR ID	DWR1	DWR3	DWR4
DWR1	1	0.857	0.803
DWR3	0.857	1	0.965
DWR4	0.803	0.965	1

TABLE 14. Correlation matrix of dominant direction θ_0 between the three DWRs. Only cases with significant wave height larger than 0.3 m and with dominant waves from northwest are considered.

DWR ID	DWR1	DWR3	DWR4
DWR1	1	0.604	0.418
DWR3	0.604	1	0.708
DWR4	0.418	0.708	1

List of Figures

1 (Color online) (a) Topography around Bjørnafjorden. This figure is plotted based on the NASA SRTM (Shuttle Radar Topography Mission) digital elevation model data. The latitude and longitudes are also marked on the map. (b) Local topography and hydrography around Bjørnafjorden. Directions of incoming waves are marked. (c) The position of three Datawell Wave Riders (DWRs) in Bjørnafjorden. Two ferry routes and approximate distances between DWRs are also marked. (Norwegian Mapping Authority Kartverket) (d) the DWR and the mooring system used in the measurement. Adapted from (DHI 2016). 44

2 The time history of measured wave elevation at three DWRs containing ship generated waves. 45

3 A general procedure for detecting and removing ship waves from measured raw wave data. 46

4 The wavelet power spectra of original and reconstructed wave elevations. 47

5 The ship generated waves obtained from wavelet and inverse wavelet analyses. . . 48

6 The power spectra of original and reconstructed wave elevation, the corresponding 95% confidence intervals (CI) are also marked. 49

7 The directional wave spectra estimated by extended maximum likelihood method (EMLM). The corresponding significant wave height is about 0.11 m. 50

8 The directional wave spectra estimated at three DWRs by the FSDM and EMLM for the case with highest significant wave height at 1 am on Aug. 9, 2016. The FSDM is used to estimate the main direction and spreading exponent s in Eq. 10, the corresponding directional wave spectra is estimated from Eq. 8. Significant wave heights at DWR1, DWR3, and DWR4 are 1.22 m, 1.12 m and 1.10 m, respectively. 51

9 Time history of wave elevation at three DWRs for the case with highest significant wave height. No ship waves are detected. 52

10 Power spectra of wave elevation at three DWRs for the case with highest significant wave height. No ship waves are detected. 53
11 The significant wave height H_s at the three DWRs, Only $H_s \geq 0.3m$ is considered. (a) is the H_s of reconstructed waves excluding ship waves, (b) is the increase of H_s due to ship waves. 54
12 The average zero up-crossing periods T_z, peak periods T_p and dominant directions θ_0 at three DWRs for different cases with significant wave height larger than 0.3 m. 55
13 The significant wave height H_s, average zero up-crossing periods T_z, and dominant directions θ_0 at three DWRs for different cases with significant wave height larger than 0.3 m and with dominant direction from northwest. 56
14 Statistical properties of significant wave height H_s at DWR1, DWR3 and DWR4, and average zero up-crossing periods T_z, and dominant direction θ_0 at DWR3. Histogram, distribution, mean and confidence interval of mean are shown. All cases with significant wave height larger than 0.3 m and with dominant direction from northwest are included. 57
15 Relative difference of significant wave height H_s, average zero up-crossing periods T_z, and dominant directions θ_0 between the DWR3 and the DWR1, DWR4. Only cases with significant wave height larger than 0.3 m and with dominant direction from northwest are considered. 58
16 Statistical properties of wave parameters. Histogram, distribution, mean and confidence interval of mean are shown. Only cases with significant wave height larger than 0.3 m and with dominant direction from northwest are considered. 59
17 The coherence of wave elevations between the three DWRs for the case with the largest significant wave height. Coh_{13} means coherence between DWR1 and DWR3, Coh_{14} denotes coherence between DWR1 and DWR4, Coh_{34} represents coherence between DWR3 and DWR4. The time series and power spectra of wave elevations at the three DWRs are shown in Fig. 9 and 10, respectively. 60

18 The mean value and standard deviation of coherence for wave elevations between different DWRs. (a) Coh_{13} between DWR1 and DWR3, (b) Coh_{14} between DWR1 and DWR4, (c) Coh_{34} between DWR3 and DWR4. Only cases with significant wave height higher than 0.3 m are considered. 61

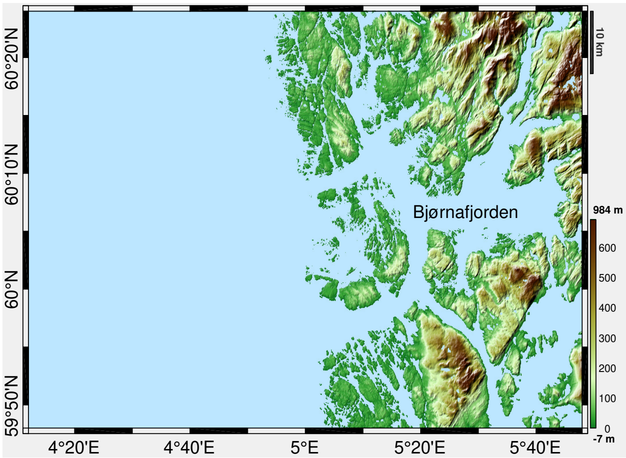

(a) Location of the Bjørnafjorden

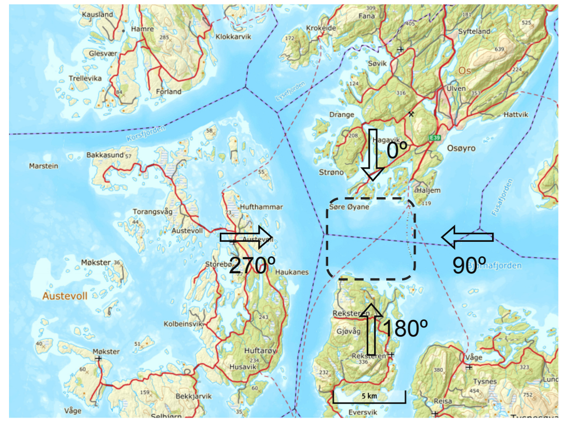

(b) The Bjørnafjorden

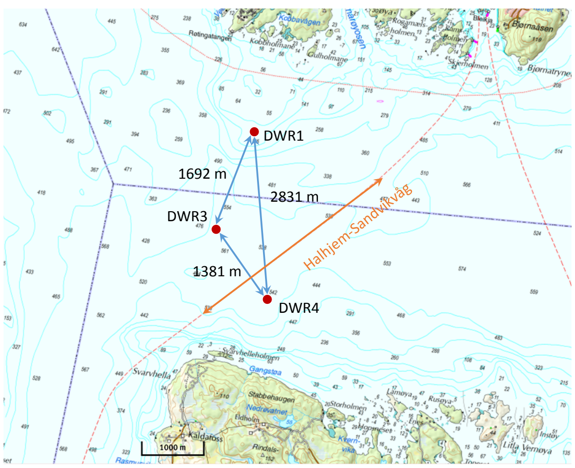

(c) Position of DWRs

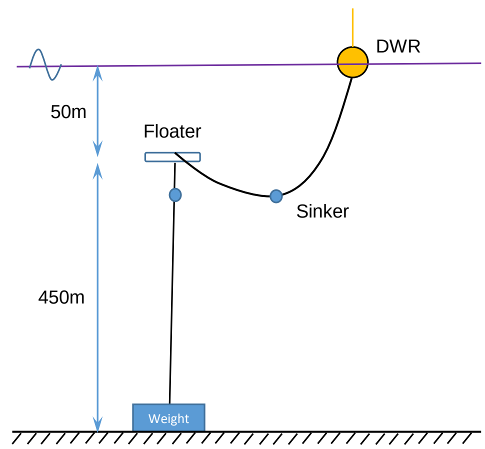

(d) Mooring system

Fig. 1. (Color online) (a) Topography around Bjørnafjorden. This figure is plotted based on the NASA SRTM (Shuttle Radar Topography Mission) digital elevation model data. The latitude and longitudes are also marked on the map. (b) Local topography and hydrography around Bjørnafjorden. Directions of incoming waves are marked. (c) The position of three Datawell Wave Riders (DWRs) in Bjørnafjorden. Two ferry routes and approximate distances between DWRs are also marked. (Norwegian Mapping Authority Kartverket) (d) the DWR and the mooring system used in the measurement. Adapted from (DHI 2016).

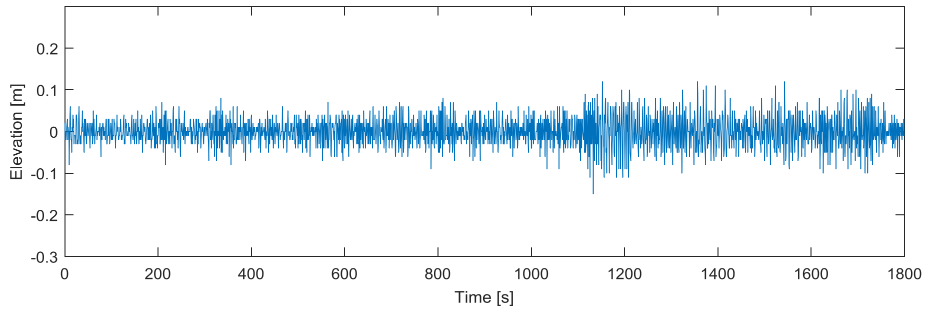

(a) DWR1

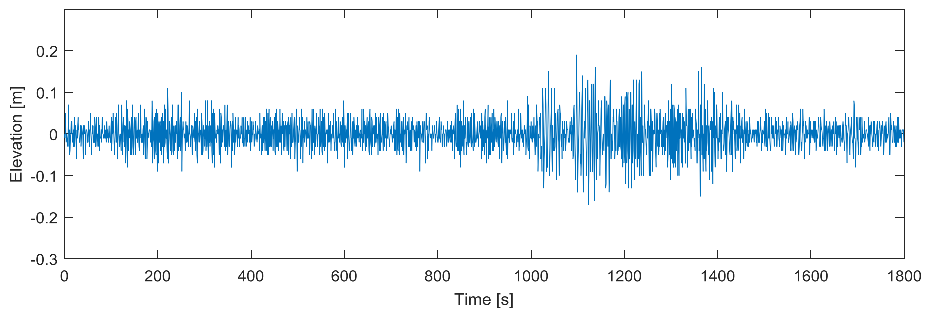

(b) DWR3

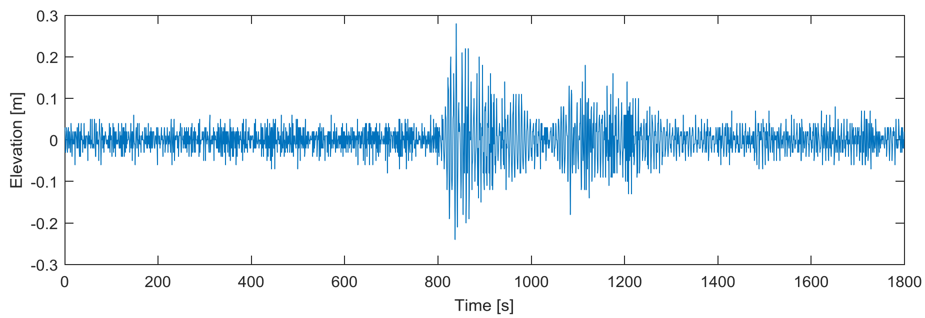

(c) DWR4

Fig. 2. The time history of measured wave elevation at three DWRs containing ship generated waves.

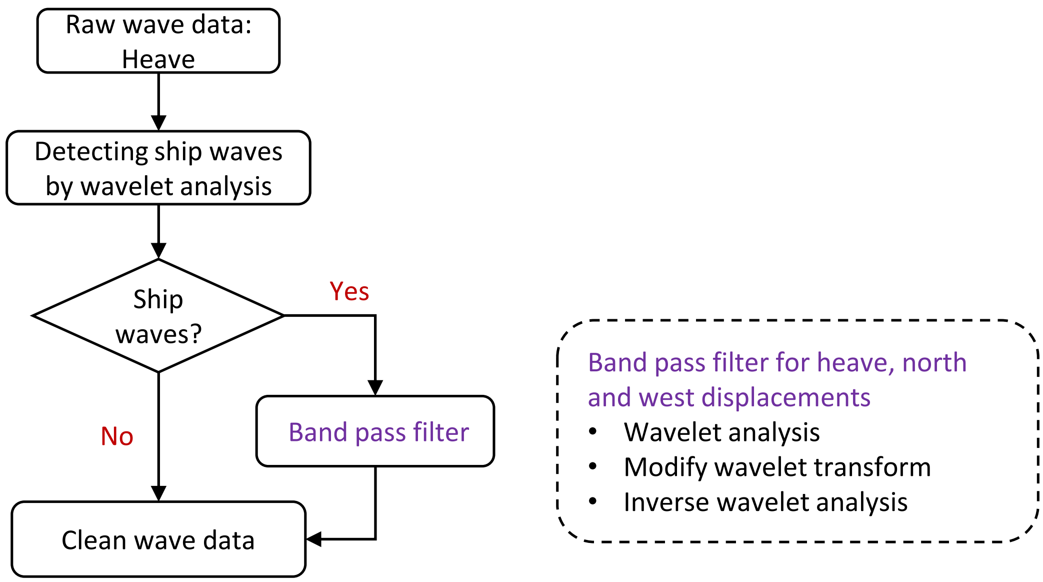

Fig. 3. A general procedure for detecting and removing ship waves from measured raw wave data.

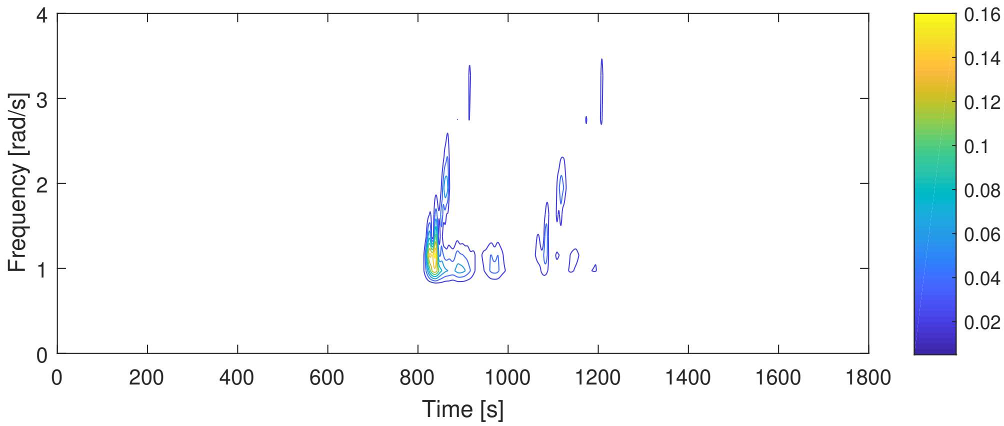

(a) Original wavelet power spectrum

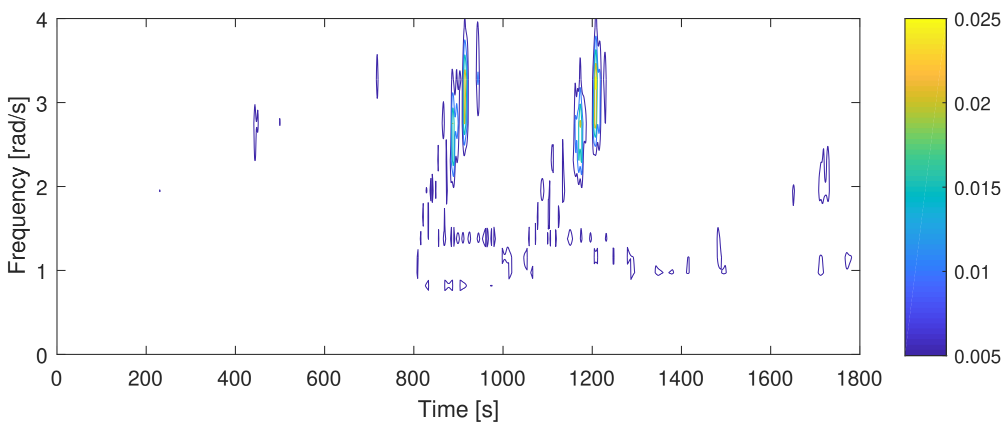

(b) Modified wavelet power spectrum

Fig. 4. The wavelet power spectra of original and reconstructed wave elevations.

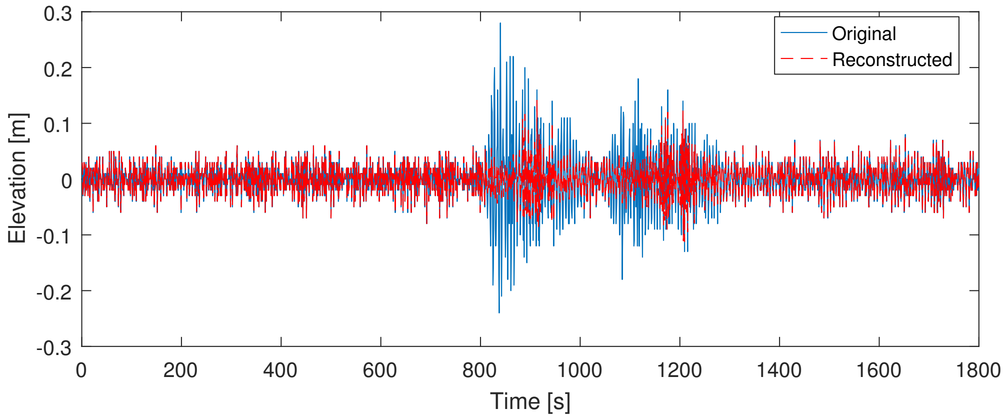

(a) Original and reconstructed wave elevations

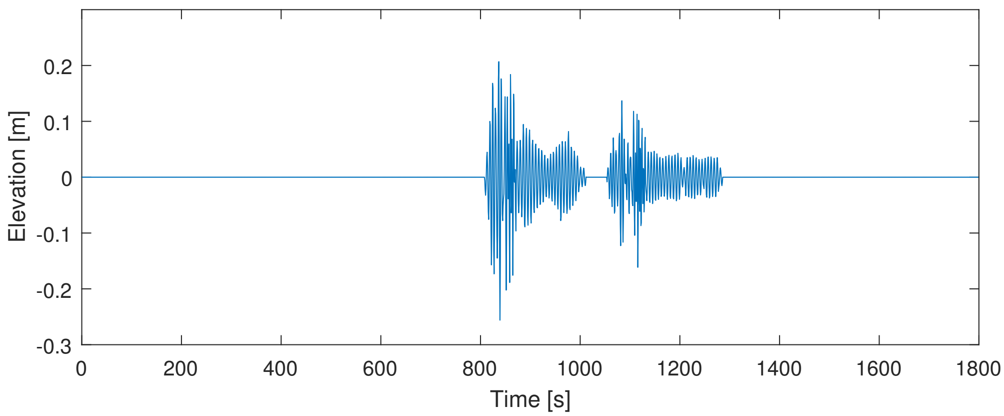

(b) Ship waves

Fig. 5. The ship generated waves obtained from wavelet and inverse wavelet analyses.

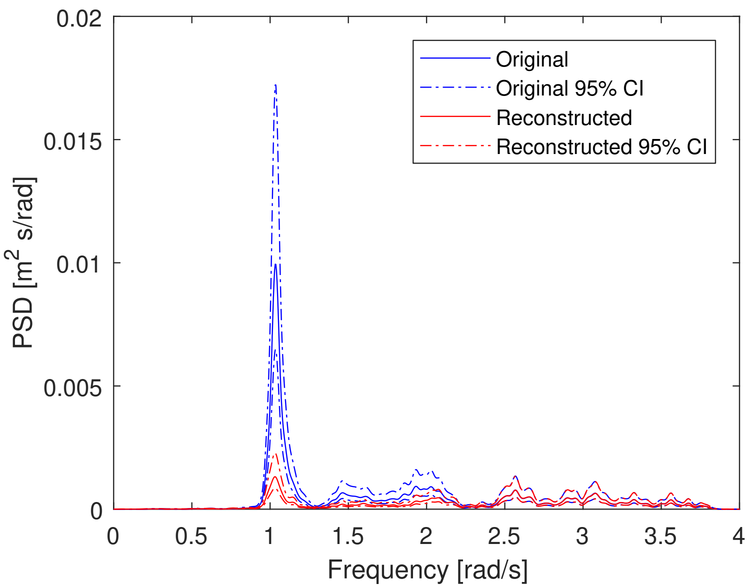

Fig. 6. The power spectra of original and reconstructed wave elevation, the corresponding 95% confidence intervals (CI) are also marked.

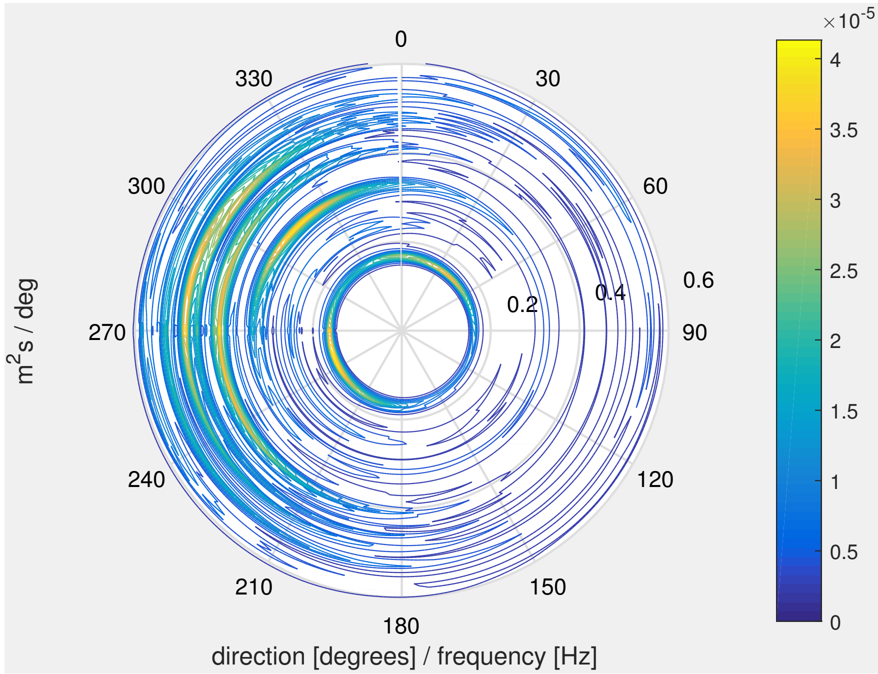

Fig. 7. The directional wave spectra estimated by extended maximum likelihood method (EMLM). The corresponding significant wave height is about 0.11 m.

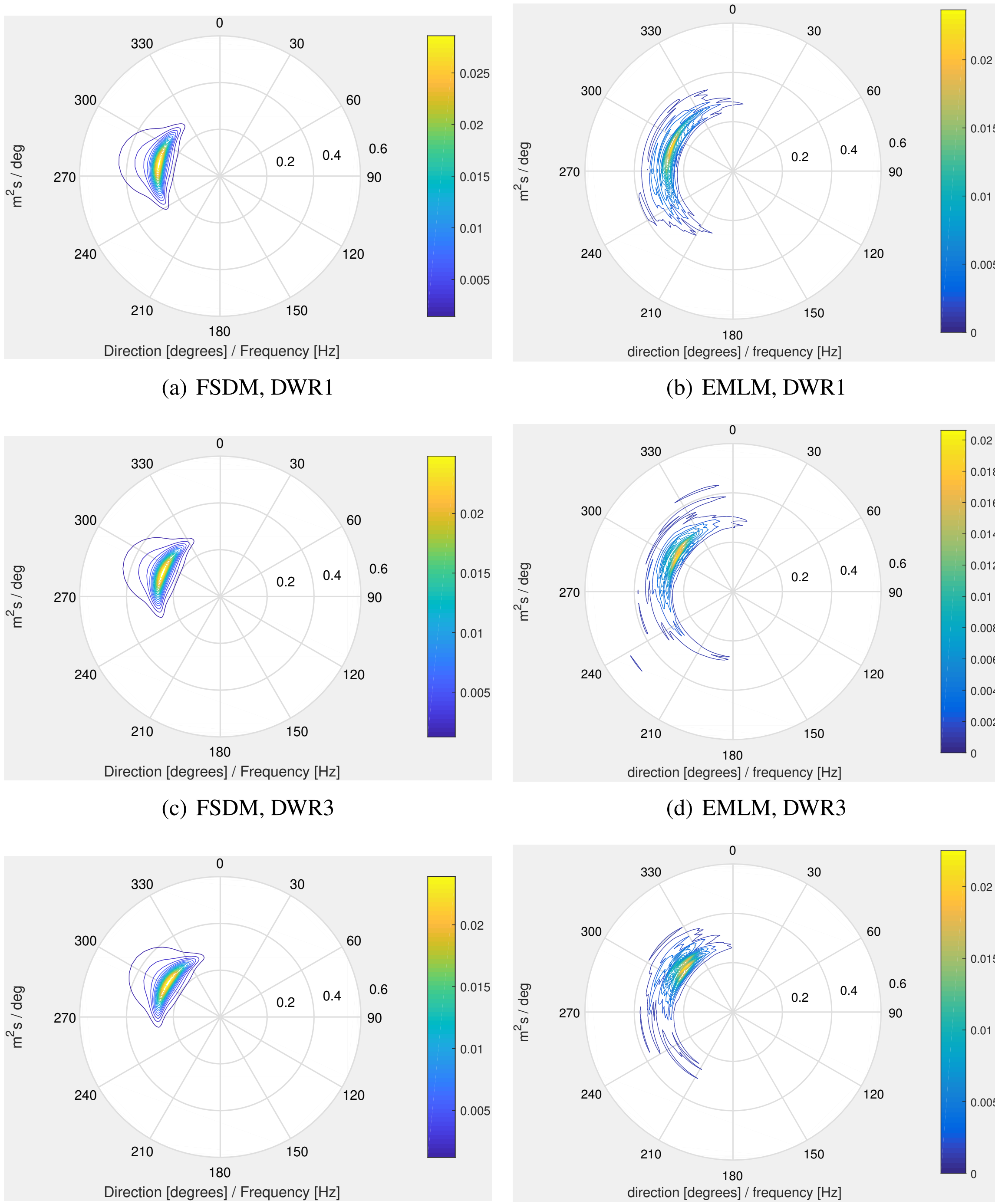

(a) FSDM, DWR1 (b) EMLM, DWR1

(c) FSDM, DWR3 (d) EMLM, DWR3

(e) FSDM, DWR4 (f) EMLM, DWR4

Fig. 8. The directional wave spectra estimated at three DWRs by the FSDM and EMLM for the case with highest significant wave height at 1 am on Aug. 9, 2016. The FSDM is used to estimate the main direction and spreading exponent s in Eq. 10, the corresponding directional wave spectra is estimated from Eq. 8. Significant wave heights at DWR1, DWR3, and DWR4 are 1.22 m, 1.12 m and 1.10 m, respectively.

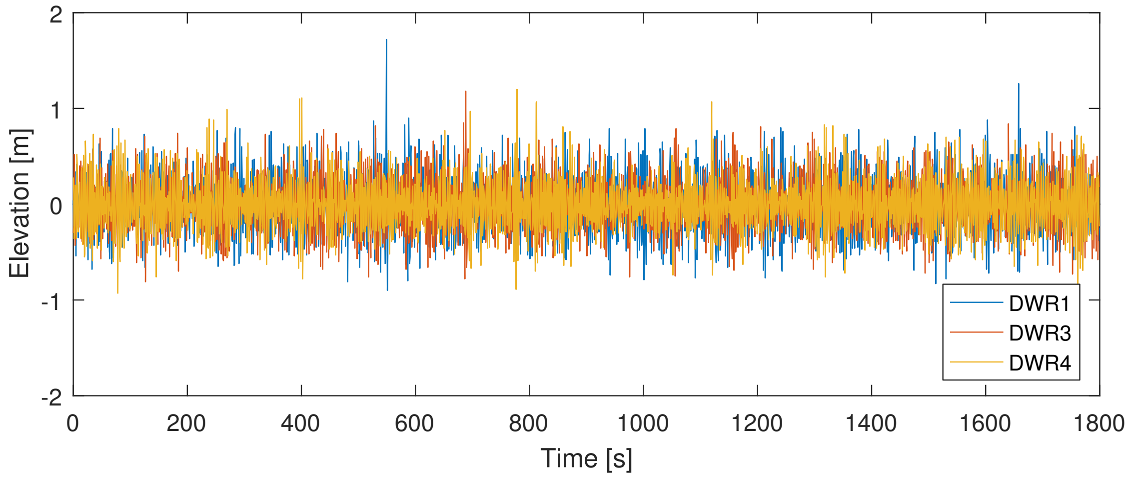

Fig. 9. Time history of wave elevation at three DWRs for the case with highest significant wave height. No ship waves are detected.

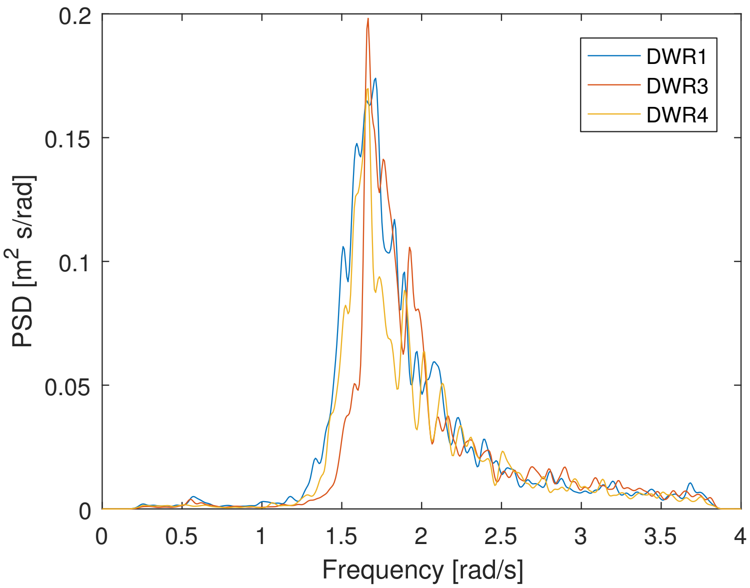

Fig. 10. Power spectra of wave elevation at three DWRs for the case with highest significant wave height. No ship waves are detected.

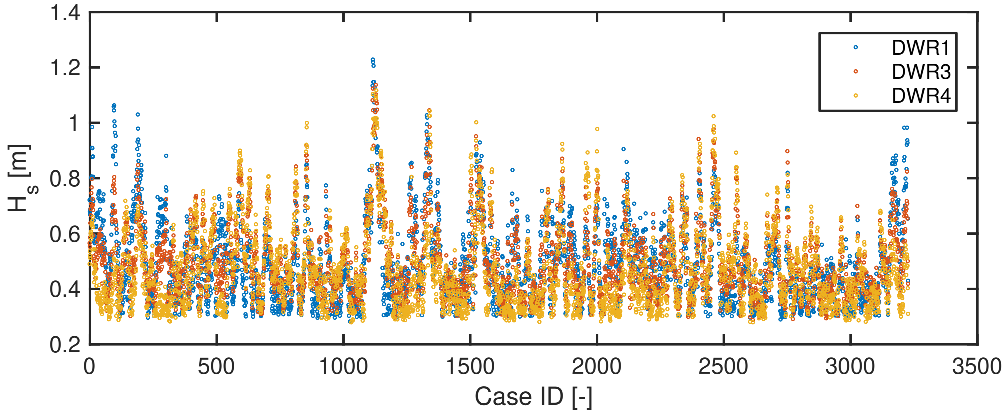

(a) H_s of reconstructed waves, Hs_{rec}.

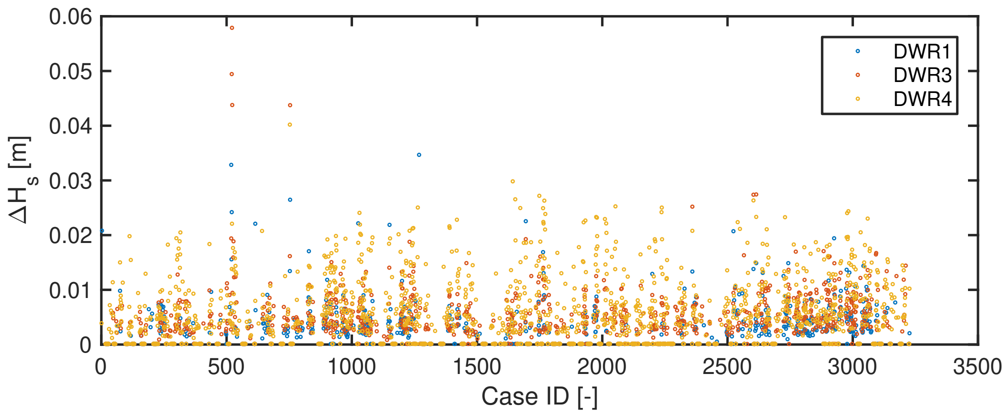

(b) increase in H_s due to ship waves, $\Delta Hs = Hs_{org} - Hs_{rec}$.

Fig. 11. The significant wave height H_s at the three DWRs, Only $H_s \geq 0.3m$ is considered. (a) is the H_s of reconstructed waves excluding ship waves, (b) is the increase of H_s due to ship waves.

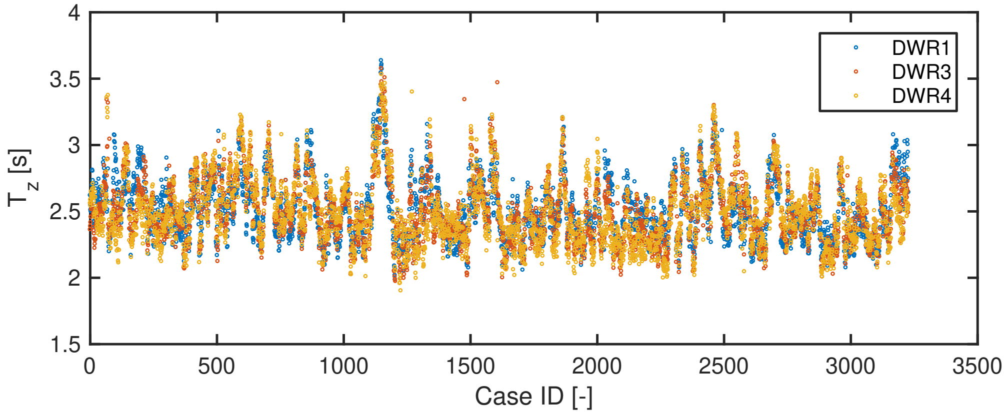

(a) Average zero up-crossing period T_z

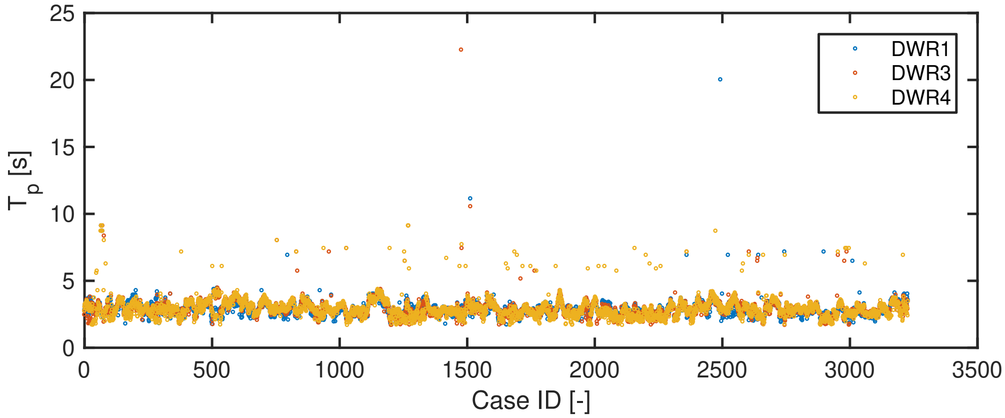

(b) Peak period T_p

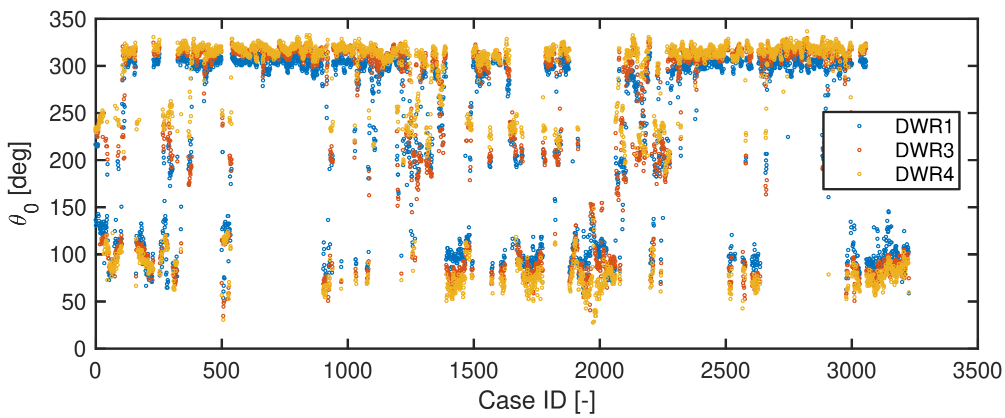

(c) Dominant direction θ_0

Fig. 12. The average zero up-crossing periods T_z, peak periods T_p and dominant directions θ_0 at three DWRs for different cases with significant wave height larger than 0.3 m.

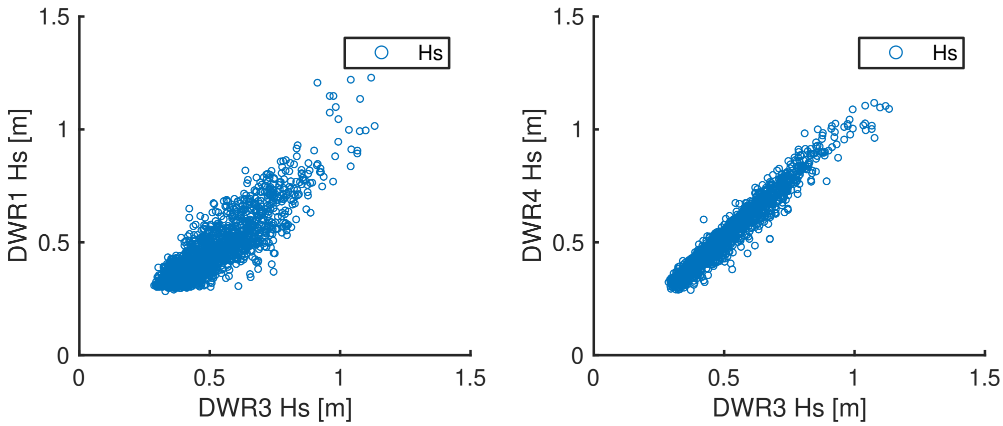

(a) Significant wave height H_s

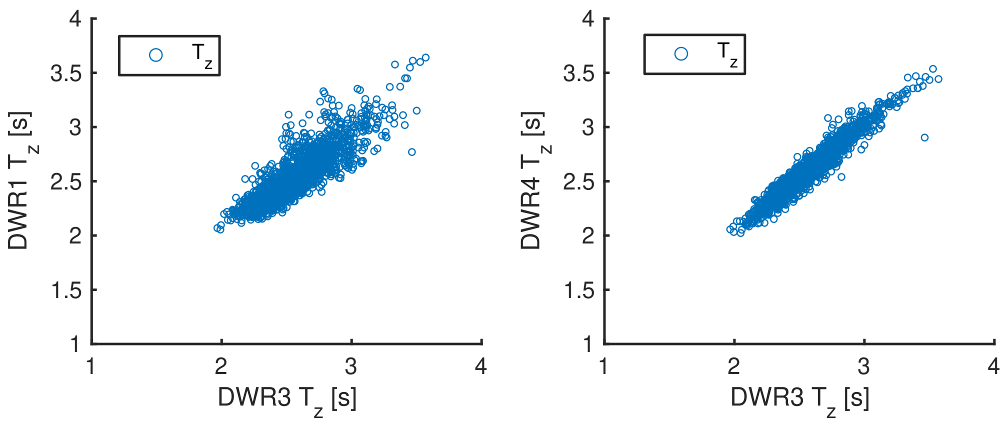

(b) Average zero up-crossing period T_z

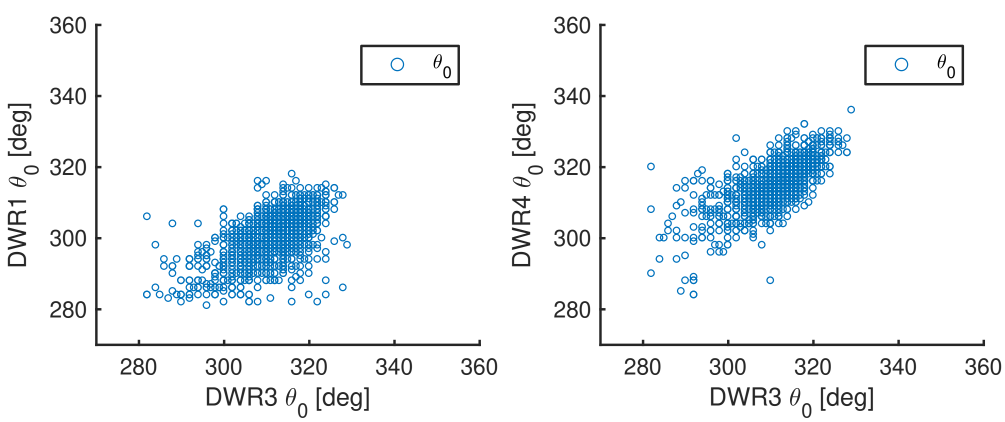

(c) Dominant direction θ_0

Fig. 13. The significant wave height H_s, average zero up-crossing periods T_z, and dominant directions θ_0 at three DWRs for different cases with significant wave height larger than 0.3 m and with dominant direction from northwest.

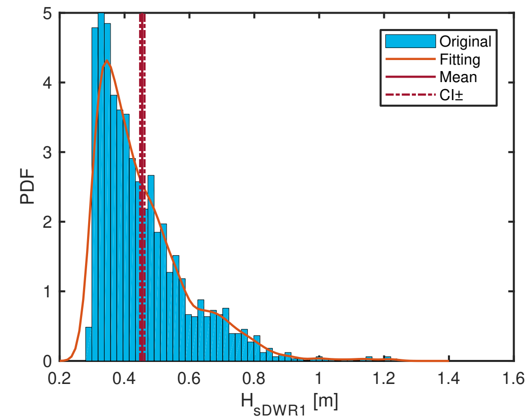

(a) Significant wave height H_s at DWR1

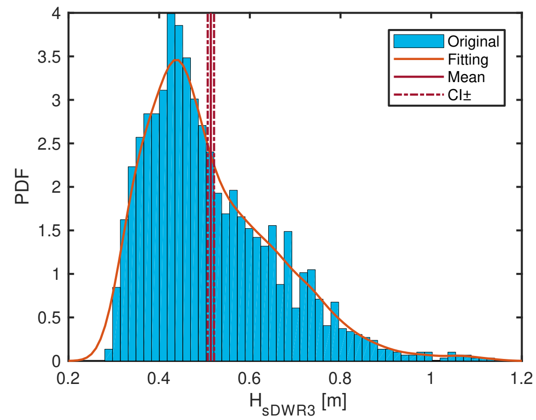

(b) Significant wave height H_s at DWR3

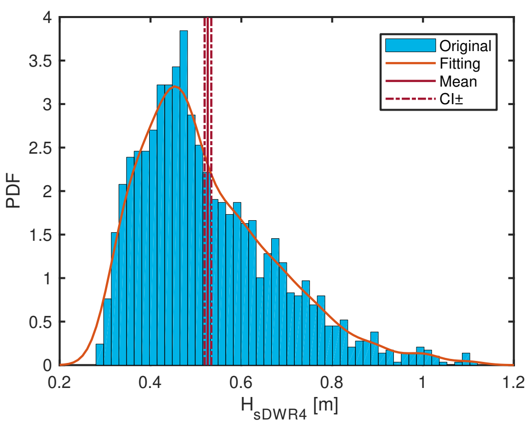

(c) Significant wave height H_s at DWR4

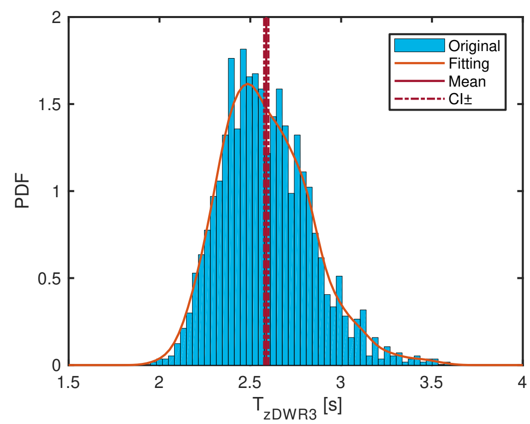

(d) Average zero up-crossing period T_z at DWR3

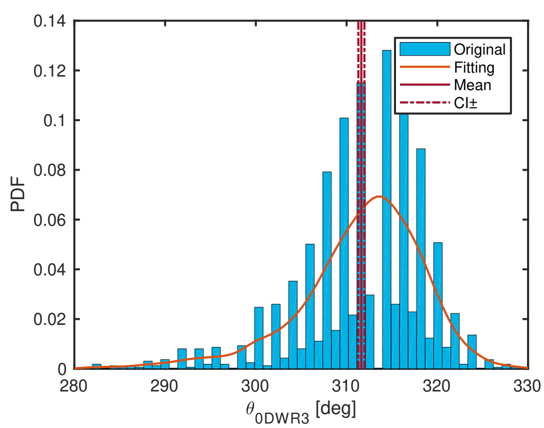

(e) Dominant direction θ_0 at DWR3

Fig. 14. Statistical properties of significant wave height H_s at DWR1, DWR3 and DWR4, and average zero up-crossing periods T_z, and dominant direction θ_0 at DWR3. Histogram, distribution, mean and confidence interval of mean are shown. All cases with significant wave height larger than 0.3 m and with dominant direction from northwest are included.

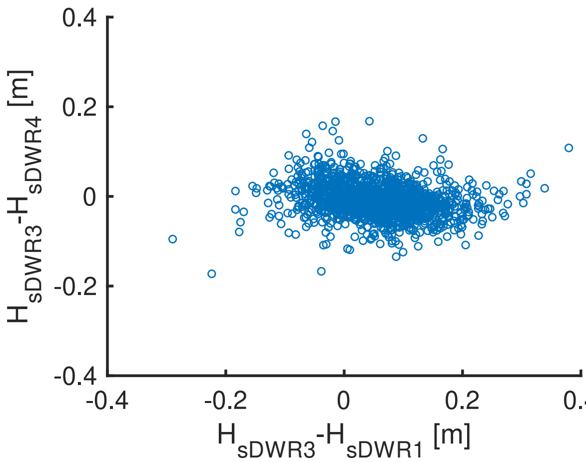

(a) Significant wave height H_s

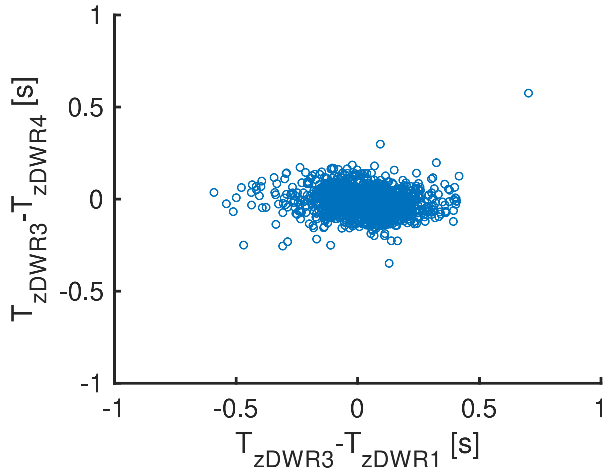

(b) Average zero up-crossing period T_z

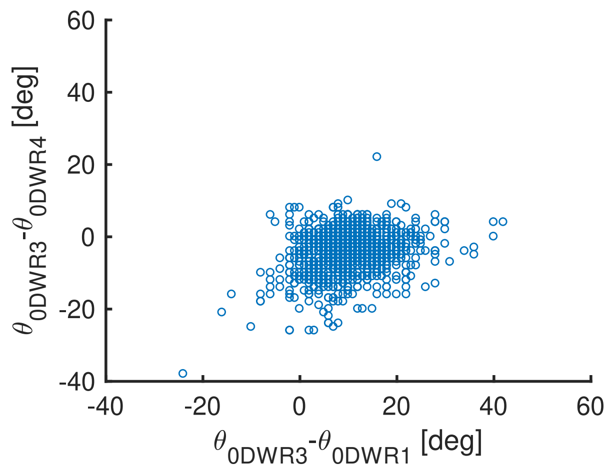

(c) Dominant direction θ_0

Fig. 15. Relative difference of significant wave height H_s, average zero up-crossing periods T_z, and dominant directions θ_0 between the DWR3 and the DWR1, DWR4. Only cases with significant wave height larger than 0.3 m and with dominant direction from northwest are considered.

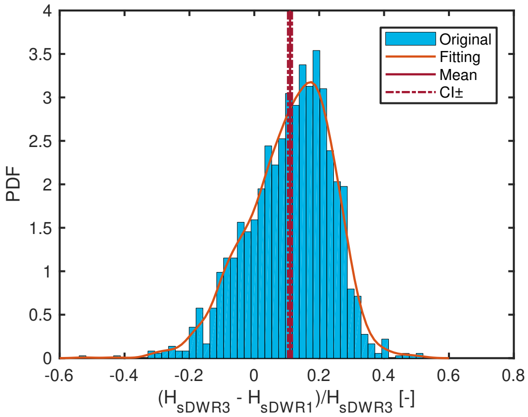

(a) $\Delta H_s = \frac{H_{sDWR3} - H_{sDWR1}}{H_{sDWR3}}$

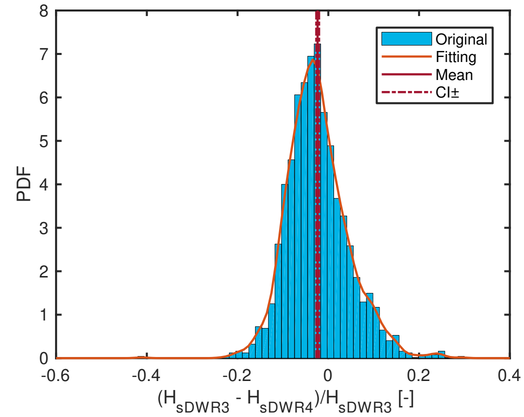

(b) $\Delta H_s = \frac{H_{sDWR3} - H_{sDWR4}}{H_{sDWR3}}$

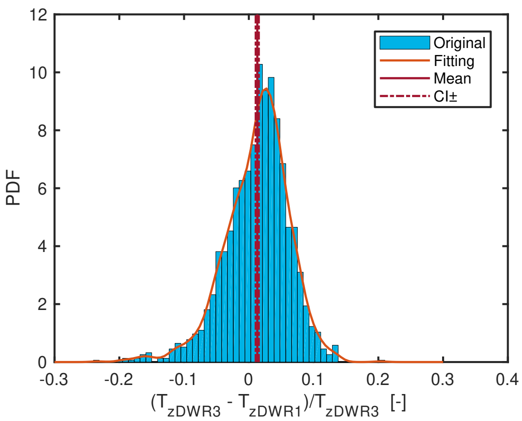

(c) $\Delta T_z = \frac{T_{zDWR3} - T_{zDWR1}}{T_{zDWR3}}$

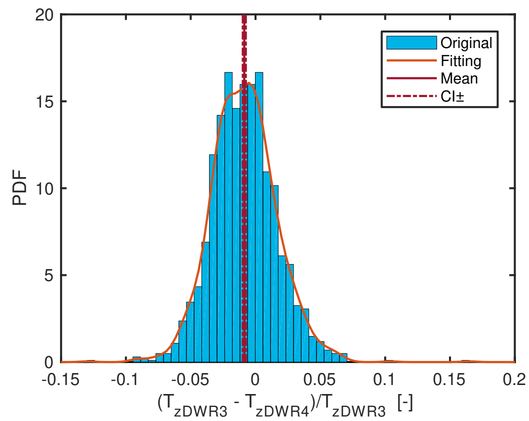

(d) $\Delta T_z = \frac{T_{zDWR3} - T_{zDWR4}}{T_{zDWR3}}$

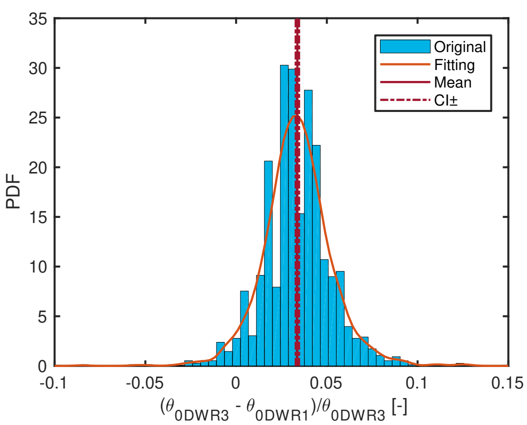

(e) $\Delta \theta_0 = \frac{\theta_{0DWR3} - \theta_{0DWR1}}{\theta_{0DWR3}}$

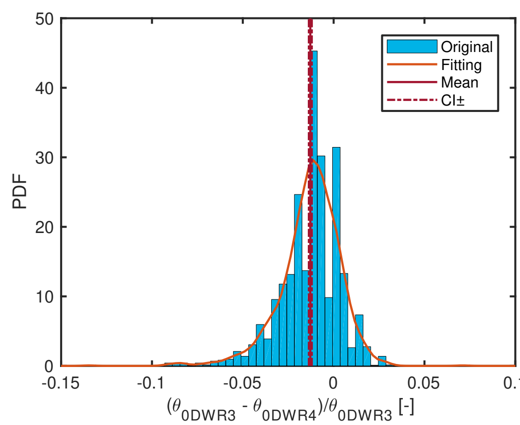

(f) $\Delta \theta_0 = \frac{\theta_{0DWR3} - \theta_{0DWR4}}{\theta_{0DWR3}}$

Fig. 16. Statistical properties of wave parameters. Histogram, distribution, mean and confidence interval of mean are shown. Only cases with significant wave height larger than 0.3 m and with dominant direction from northwest are considered.

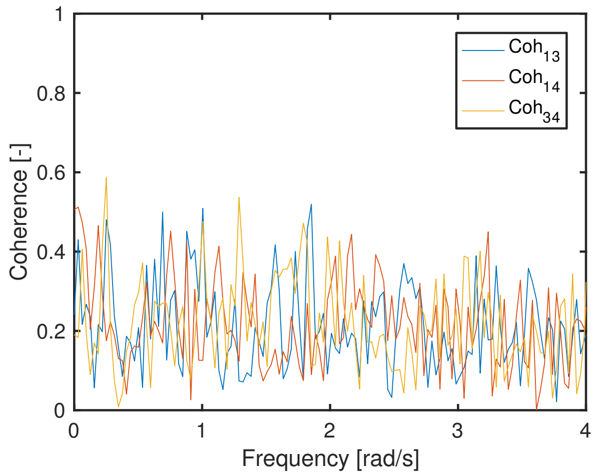

Fig. 17. The coherence of wave elevations between the three DWRs for the case with the largest significant wave height. Coh_{13} means coherence between DWR1 and DWR3, Coh_{14} denotes coherence between DWR1 and DWR4, Coh_{34} represents coherence between DWR3 and DWR4. The time series and power spectra of wave elevations at the three DWRs are shown in Fig. 9 and 10, respectively.

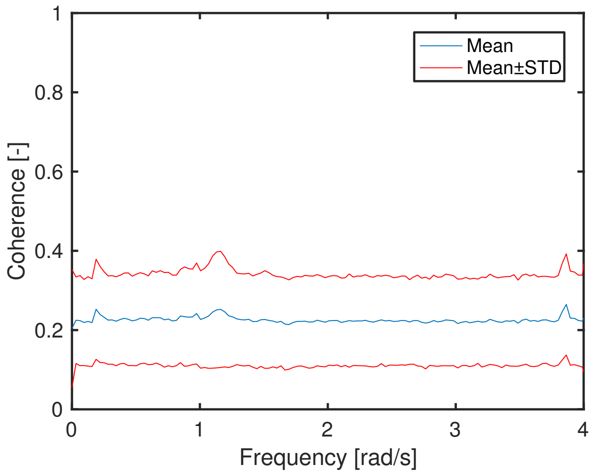

(a) Coh_{13} between DWR1 and DWR3

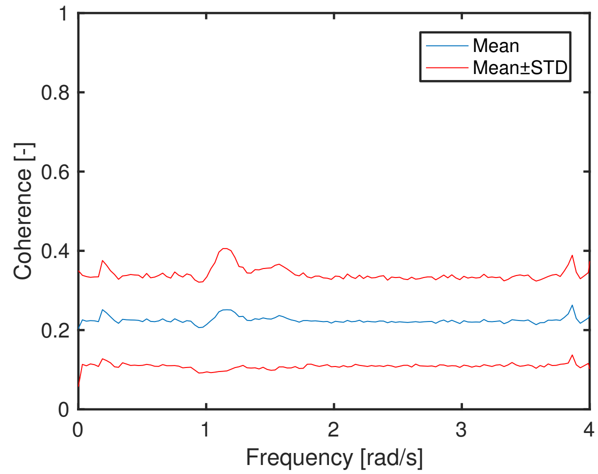

(b) Coh_{14} between DWR1 and DWR4

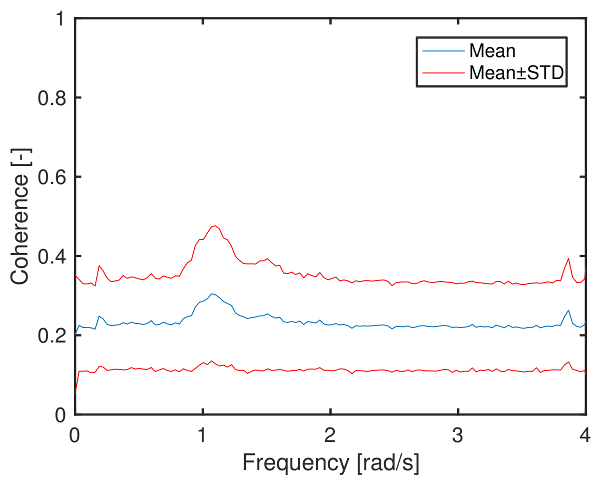

(c) Coh_{34} between DWR3 and DWR4

Fig. 18. The mean value and standard deviation of coherence for wave elevations between different DWRs. (a) Coh_{13} between DWR1 and DWR3, (b) Coh_{14} between DWR1 and DWR4, (c) Coh_{34} between DWR3 and DWR4. Only cases with significant wave height higher than 0.3 m are considered.